Mon. Not. R. Astron. Soc. **390,** 881–905 (2008) doi:10.1111/j.1365-2966.2008.13713.x

Photometric characterization of a well-defined sample of isolated galaxies in the context of the AMIGA project

A. Durbala,[1★] J. W. Sulentic,[1] R. Buta[1] and L. Verdes-Montenegro[2]

[1]*Department of Physics and Astronomy, University of Alabama, Box 870324, Tuscaloosa, AL 35487-0324, USA*
[2]*Instituto de Astrofísica de Andalucía, CSIC, Apdo. 3004, 18080 Granada, Spain*

Accepted 2008 July 12. Received 2008 July 5; in original form 2008 May 29

ABSTRACT

We perform a detailed photometric analysis (bulge–disc–bar decomposition and Concentration-Asymmetry-Clumpiness – CAS parametrization) for a well-defined sample of isolated galaxies, extracted from the Catalog of Isolated Galaxies and reevaluated morphologically in the context of the Analysis of the interstellar Medium of Isolated GAlaxies project. We focus on Sb–Sc morphological types, as they are the most representative population among the isolated spiral galaxies. Our analysis yields a large number of important galactic parameters and various correlation plots are used to seek relationships that might shed light on the processes involved in determining those parameters. Assuming that the bulge Sérsic index and/or bulge/total luminosity ratios are reasonable diagnostics for pseudo- versus classical bulges, we conclude that the majority of late-type isolated disc galaxies likely host pseudo-bulges rather than classical bulges. Our parametrization of galactic bulges and discs suggests that the properties of the pseudo-bulges are strongly connected to those of the discs. This may indicate that pseudo-bulges are formed through internal processes within the discs (i.e. secular evolution) and that bars may play an important role in their formation. Although the sample under investigation covers a narrow morphological range, a clear separation between Sb and Sbc–Sc types is observed in various measures, e.g. the former are redder, brighter, have larger discs and bars, more luminous bulges, are more concentrated, more symmetric and clumpier than the latter. A comparison with samples of spiral galaxies (within the same morphological range) selected without isolation criteria reveals that the isolated galaxies tend to host larger bars, are more symmetric, less concentrated and less clumpy.

Key words: galaxies: bulges – galaxies: evolution – galaxies: fundamental parameters – galaxies: general – galaxies: photometry – galaxies: structure.

1 INTRODUCTION

The properties of galaxies and their evolution are thought to be strongly related to their environment. The empirical quantification of environmental influence (‘nurture’) on morphology, structure, nuclear activity, star formation properties, etc. requires a robust definition of a sample of galaxies that are minimally perturbed by other galaxies. Such a sample could serve as a ‘pure nature’ baseline. In this sense, perhaps the best compilation of isolated galaxies available at this time is the Catalog of Isolated Galaxies (CIG; Karachentseva 1973). Both the size (n = 1050 galaxies) and the restrictive isolation criteria in the catalogue contribute to its statistical value. The definition of isolation requires that, for a galaxy of diameter D, there is no companion/neighbour with a diameter d in the range D/4 to 4D within a distance of 20D. The isolation criteria used to construct the CIG suggest that a typical galaxy of 25 kpc diameter has not been visited by a similar mass perturber in the past ∼3 Gyr (assuming a typical field velocity of ∼150 km s^{-1}; Verdes-Montenegro et al. 2005). Thus, the evolution of such isolated galaxies is mostly driven by internal processes and to a much lesser degree by environment, at least for the last ∼3 Gyr of their existence.

A recent morphological reevaluation of the CIG galaxies in the context of the Analysis of the interstellar Medium of Isolated GAlaxies project (AMIGA) revealed that the bulk (∼63 per cent) shows morphological types in the range Sb–Sc (Sulentic et al. 2006). In this study, we present the results of a photometric characterization for a representative subsample of $n \sim 100$ CIG galaxies classified as Sb–Sc in this latter reference. We perform multicomponent decomposition (bulge/disc/bar) using the BUDDA code[1] (de Souza, Gadotti

★E-mail: adriana.durbala@ua.edu

[1] http://www.mpa-garching.mpg.de/ dimitri/budda.html

& dos Anjos 2004). Additionally, we evaluate CAS parameters Concentration(C)–Asymmetry(A)–Clumpinesss(S) (e.g. Bershady, Jangren & Conselice 2000; Conselice, Bershady & Jangren 2000; Conselice 2003; Taylor-Mager et al. 2007). Assembling a set of parameters combining a model-dependent description of the main components of galaxies (BUDDA) with global structural measures (CAS) could provide valuable hints into the formation and evolution of galaxies.

This is the first attempt to date to present a detailed examination of this kind (bulge–disc–bar decomposition combined with CAS parameters) for a well-defined sample of isolated galaxies. This study is an integral part of the AMIGA project, which is a dedicated multiwavelength study of the revised CIG catalogue. The goal of AMIGA is to quantify the fundamental properties of a statistically meaningful sample of isolated galaxies, which can then be used as a baseline for comparison and estimation of the effects of environment in other less isolated samples of galaxies. The CIG catalogue has recently been reevaluated in terms of galaxy positions (Leon & Verdes-Montenegro 2003), isolation (Verley et al. 2007a,b) and morphology (Sulentic et al. 2006). A series of studies were produced in the context of the AMIGA project: (i) an optical characterization of the refined sample (Verdes-Montenegro et al. 2005), (ii) an analysis of mid- and far-infrared (far-IR) properties (Lisenfeld et al. 2007), (iii) a study of the neutral CO and H I gas (Espada et al. 2005; Espada 2006), (iv) radio continuum emission (Leon et al. 2008) and (v) nuclear activity (Sabater et al. 2008). Another recent study used a subsample of isolated AMIGA galaxies to investigate the role of bars in star formation processes (e.g. Verley et al. 2007c). Our present study offers a detailed photometric analysis of a representative sample of the core AMIGA population of Sb–Sc morphological types. We should note that all data produced within the AMIGA project are periodically updated and made publicly available at http://www.iaa.es/AMIGA.html.

Theoretical models and numerical simulations exploring the formation and evolution of galaxies rely on empirical results that could separate and quantify the relative roles of internal secular processes (that develop on time-scales much longer than the galaxy formation/collapse process itself) and slow or fast external perturbations (environment) in defining the structural properties of galaxies. In this sense, our present study has a two-fold importance: (i) it explores a representative and well-defined sample of *the most isolated galaxies* in the local Universe and (ii) provides an *extensive photometric structural analysis* of these galaxies. Our main goal is to identify potential scaling relations and correlations: (i) between parameters describing the same structural component (bulge, disc or bar), (ii) between components, (iii) between components and global properties of the galaxy (morphological type, colour, luminosity, concentration, asymmetry, clumpiness, etc.). With such correlations available one could explore, for example, the nature of bulges in isolated galaxies and how they are formed, the role of bars (if any) in the formation/evolution of bulges, whether the isolated spiral galaxies are different relative to spirals in richer environments in terms of global properties and/or in terms of properties of their components (bulge, bar and discs).

This paper is organized as follows: Section 2 presents the selection and basic properties of the sample, Section 3 offers a concise view on data reduction, Sections 4 and 5 present the results of BUDDA decomposition analysis and CAS parametrization, respectively. Section 6 combines various measures obtained from the BUDDA code with CAS parameters. Section 7 is dedicated to discussion and conclusions. Throughout the paper, we use $H_0 = 75$ km s^{-1} Mpc^{-1}.

2 THE SAMPLE

2.1 Sample selection

Galaxies of morphological types Sb–Sc were found to be the most abundant (dominant) population in the AMIGA reanalysis of the CIG (Sulentic et al. 2006), Sb–Sc galaxies represent 2/3 ($n \sim 637$) of the 1018 galaxies with recession velocity $V_{\rm R} > 1000$ km s^{-1}. This motivated us to focus on the Sb–Sc morphological range since earlier and later types are so rare that they cannot be considered representatives of an isolated sample. The sample adopted here was drawn from that Sb–Sc population (Sulentic et al. 2006) after applying the following constraints: (i) $1500 < V_{\rm R} < 10\,000$ km s^{-1}, (ii) blue-corrected magnitudes (Verdes-Montenegro et al. 2005) $m_{\rm Bcorr} < 15$, (iii) inclination $<70°$ and (iv) available images in Sloan Digital Sky Survey (SDSS) (Data Release 6: DR6, Adelman-McCarthy et al. 2008). We ended up with a representative sample of $n = 101$ Sb–Sc galaxies, all having SDSS *i*-band magnitudes brighter than 15. The lower limit to the $V_{\rm R}$ range avoids inclusion of local supercluster galaxies where the degree of isolation is most uncertain. The upper limit ensures a large enough SDSS overlap sample and at the same time adequate resolution to permit evaluation of basic structural parameters for all of the galaxies. We are preparing a complementary Fourier analysis of spiral structure in the same sample considered here. The need for a sufficiently accurate deprojection of galaxies in the context of the Fourier analysis requires the third constraint on inclination for the sample selection. The results of the Fourier analysis will be reported in a later paper.

SDSS images are obtained with a dedicated 2.5-m telescope (Gunn et al. 2006). The imaging process is carried out under photometric conditions (Hogg et al. 2001) in five filters (*ugriz*) (Fukugita et al. 1996; Smith et al. 2002) employing a wide-field CCD camera (Gunn et al. 1998). Data are processed by completely automated pipelines that detect and measure photometric properties of objects and astrometrically calibrate the data (Lupton et al. 2001; Pier et al. 2003).

Table 1 presents the sample of CIG galaxies that we analyse here in terms of coordinates (Leon & Verdes-Montenegro 2003), recession velocity (Verdes-Montenegro et al. 2005), morphological type from Sulentic et al. (2006) and inclination, which was estimated using the formula cos $(i) = b/a$, where a and b are the semimajor and semiminor axes of the disc, respectively. Morphological reevaluation of all CIG galaxies (Sulentic et al. 2006) was based on the second Palomar Observatory Sky Survey POSSII with some confirmation using SDSS-DR3. DR6 provides a much larger number of CIG galaxies with SDSS images. Therefore, we decided to do a SDSS-based morphological classification of our target sample of 101 galaxies in the framework presented in 'The de Vaucouleurs Atlas of Galaxies' (Buta, Corwin & Odewahn 2007). The last column of Table 1 shows our revised and more complete (visual) classification. Four galaxies (CIG: 250, 291, 308 and 392) have been excluded from our sample because they are not in the range Sb–Sc according to our revised classification (see the last four lines of Table 1). Hereafter, we consider the $N = 97$ confirmed Sb–Sbc–Sc galaxies.

2.2 Basic properties of the sample

Figs 1(a)–(d) present some basic properties of our sample (the measures shown in panels (a), (c) and (d) are based upon photometric estimates reported within the SDSS photo-pipeline): (a) distribution of galactic size, as indicated by a^i_{25}, i.e. the semimajor axis of

Table 1. CIG/KIG galaxies in our sample.

Galaxy KIG name	UGC/NGC name	RA (J2000) (hh mm ss.ss)	Dec. (J2000) (+dd mm ss.s)	v_r (km s^{-1})	i (°)	Morphological type old^i	Morphological type revised
KIG 11	UGC 00139	00 14 31.88	−00 44 10.4	3963	66	Sbc	SA(s)c
KIG 33	UGC 00461/NGC 0237	00 43 27.81	−00 07 26.9	4175	55	Sb	SA(s)c
KIG 56	UGC 01143/NGC 0622	01 36 00.13	+00 39 48.8	5155	43	Sb	SB(rs)b
KIG 187	UGC 03825	07 23 33.16	+41 26 05.6	8281	25	Sc	SAB(s)bc
KIG 198	UGC 03935	07 37 49.45	+46 23 52.4	9628	32	Sc	SAB(s)c
KIG 203		07 44 36.40	+38 02 39.6	7998	65	Sc	SA(s)c
KIG 217	UGC 04107	07 57 01.84	+49 34 02.1	3504	25	Sc	SA(rs)bc
KIG 222	UGC 04158/NGC 2503	08 00 36.75	+22 24 00.8	5506	28	Sb	SAB(s)b
KIG 232	UGC 04256/NGC 2532	08 10 15.20	+33 57 22.5	5260	30	Sc	SA(rs)c
KIG 238	UGC 04283	08 14 22.05	+39 15 05.3	8295	18	Sb	(R'_1)SB(s)b
KIG 241		08 19 15.77	+19 18 48.0	5681	46	Sc	SA(s)c
KIG 242		08 19 22.31	+23 44 50.0	4603	54	Sb	SA(s)bc
KIG 258		08 31 49.40	+28 32 11.0	6047	52	Sb	SAB(rs)b
KIG 260	UGC 04456	08 32 03.53	+24 00 38.5	5488	11	Sc	SAB(r)c
KIG 271	UGC 04512	08 39 39.91	+60 58 07.7	7911	58	Sc	SAB(s)c
KIG 281	UGC 04555/NGC 2649	08 44 08.30	+34 43 01.8	4244	32	Sc	SA(rs)bc
KIG 282	NGC 2651	08 43 55.12	+11 46 15.5	8696	34	Sc	SAB(s)bc
KIG 287	UGC 04624	08 50 23.58	+25 57 14.5	8297	58	Sbc	SAB(rs)bc
KIG 292	UGC 04708/NGC 2712	08 59 30.53	+44 54 51.5	1818	58	Sb	SA(s)b
KIG 298	UGC 04770/NGC 2746	09 05 59.41	+35 22 38.3	7065	29	Sb	SB(rs)b
KIG 302	NGC 2761	09 07 30.76	+18 26 05.2	8728	55	Sc	SA(s)c
KIG 314	UGC 04838/NGC 2776	09 12 14.37	+44 57 17.8	2626	8	Sc	SA(rs)c
KIG 322		09 21 10.80	+45 53 17.4	1858	22	Sc	SA(rs)c
KIG 325	UGC 04973	09 22 38.12	+60 51 55.6	7823	21	Sc	SAB(s)bc
KIG 328	UGC 05002	09 24 22.90	+28 17 34.9	6518	42	Sbc	SAB(s)bc
KIG 330		09 25 30.87	+45 31 57.2	4276	43	Sbc	SAB(s)bc
KIG 336	UGC 05038	09 27 23.45	+30 26 26.5	8070	32	Sb	(R'_1)SB(r)b
KIG 339	UGC 05055	09 30 11.77	+55 51 07.4	7540	32	Sbc	(R'_2)SB(s)bc
KIG 351		09 35 21.80	+13 32 55.9	5920	42	Sb	SB(rs)b
KIG 365		09 42 31.53	+07 05 57.1	8627	27	Sc	SAB(rs)b
KIG 366	UGC 05184	09 43 02.20	+37 49 22.3	6581	53	Sb	SB(s)b
KIG 367	UGC 05201	09 44 34.94	+55 45 48.3	7627	51	Sc	SA(s)c
KIG 368		09 44 47.09	+51 41 19.5	9959	25	Sc	SA(s)c
KIG 386		09 57 48.95	+51 49 16.7	7490	49	Sc	SAB(s)c
KIG 397	UGC 05425/NGC 3107	10 04 22.53	+13 37 18.1	2791	44	Sb	SAB(s)bc
KIG 399		10 07 50.53	+34 18 56.5	6106	40	Sc	SA(s)bc
KIG 401	UGC 05472	10 08 32.01	−00 39 57.2	6436	55	Sbc	SB(rs)bc
KIG 405	UGC 05521	10 13 52.60	+00 33 03.0	6232	28	Sc	SAB(s)c
KIG 406		10 14 08.03	+10 08 54.5	8355	49	Sc	SA(s)c
KIG 409		10 22 00.37	+25 52 20.1	6371	40	Sbc	SAB(s)bc
KIG 410	UGC 05606	10 22 24.06	+01 11 55.1	6492	36	Sbc	SA(s)bc
KIG 429		10 39 45.32	+11 38 49.8	8991	42	Sc	SAB(s)c
KIG 444	UGC 05956	10 50 58.37	−02 09 00.6	4469	13	Sb	SA$\underline{\text{B}}$(s)c
KIG 446		10 52 25.05	+59 41 08.9	8417	44	Sc	SA(rs)bc
KIG 460		11 05 00.56	+14 53 43.8	6186	52	Sb	SAB(s)bc
KIG 466	UGC 06194	11 09 00.70	+22 55 45.4	2643	26	Sc	(R'_2)SAB(s)c
KIG 489	UGC 06568	11 35 36.88	+00 07 38.6	5910	56	Sbc	SA(s)c
KIG 491	UGC 06608	11 38 33.25	−01 11 05.2	6251	48	Sc	SA(rs)bc
KIG 494		11 40 39.23	+28 51 49.3	6825	24	Sbc	SAB(s)c
KIG 499	UGC 06769	11 47 43.71	+01 49 34.1	8537	62	Sbc	SAB(r)b
KIG 502	UGC 06780	11 48 50.37	−02 01 57.5	1729	70	Sbc	SA(s)c
KIG 508	UGC 06854	11 52 43.45	+01 44 27.0	6128	29	Sbc	SAB(s)c
KIG 512	UGC 06903	11 55 36.90	+01 14 13.5	1892	28	Sc	SB(s)c
KIG 515		11 58 36.22	+18 51 47.6	6876	60	Sbc	SAB(s)c
KIG 520	UGC 07144	12 09 45.08	+56 31 26.8	7864	33	Sc	SAB(rs)bc
KIG 522		12 15 40.77	+61 53 22.6	6102	34	Sb	SB(rs)b
KIG 525	UGC 07416	12 21 39.18	+40 50 54.9	6901	22	Sb	SB(r)b
KIG 532		12 31 34.55	+37 58 47.9	7129	39	Sb	SAB(rs)c
KIG 550	UGC 07917/NGC 4662	12 44 26.17	+37 07 17.1	6985	25	Sbc	SB(r)b
KIG 553	UGC 07987/NGC 4719	12 50 08.69	+33 09 33.0	7091	28	Sb	SB(r)b
KIG 560		12 56 53.52	+22 22 24.7	6529	38	Sc	(R'_1)S$\underline{\text{A}}$B(s)c
KIG 571	UGC 08184/NGC 4964	13 05 24.69	+56 19 24.7	2520	54	Sc	SA(s)c
KIG 575	UGC 08279/NGC 5016	13 12 06.63	+24 05 42.2	2612	42	Sb	SA(rs)c

Table 1 – *continued*

Galaxy KIG name	UGC/NGC name	RA (J2000) (hh mm ss.ss)	Dec. (J2000) (+dd mm ss.s)	v_r (km s^{-1})	i (°)	Morphological type old[i]	revised
KIG 580		13 19 01.90	+14 47 28.0	6643	57	Sbc	SA(s)c
KIG 598	UGC 08705	13 46 32.29	+20 50 51.3	6938	58	Sc	SAB(s)bc
KIG 600		13 49 28.89	+13 52 36.5	7228	41	Sc	(R'_2)SA(rs)c
KIG 612	UGC 09035	14 07 55.41	+29 52 22.2	8244	28	Sbc	SB(rs)b
KIG 626	UGC 09201/NGC 5584	14 22 23.67	−00 23 14.1	1640	45	Sc	SAB(s)c
KIG 630	UGC 09248/NGC 5622	14 26 12.18	+48 33 50.4	3861	58	Sb	SA(s)b
KIG 633		14 32 27.42	+27 25 38.3	4298	29	Sbc	SA(s)bc
KIG 639		14 37 49.61	+06 44 54.1	8659	52	Sc	SA(s)c
KIG 640		14 38 38.22	+54 16 40.4	8790	24	Sbc	SA(s)bc
KIG 641	UGC 09461	14 39 33.01	+62 00 10.5	6728	45	Sb	SB(r)b
KIG 645	UGC 09516	14 45 48.85	+50 23 38.5	4027	35	Sc	(R_2)SA(s)c
KIG 652	UGC 09564/NGC 5768	14 52 08.05	−02 31 47.9	1962	27	Sc	SAB(s)bc
KIG 665		15 12 24.98	+18 38 47.7	6408	54	Sb	SA(s)b
KIG 671	UGC 09826	15 21 33.05	+39 12 04.3	8822	11	Sb	SAB(rs)b
KIG 689		15 36 36.23	+17 20 17.5	4292	58	Sbc	SB(s)c
KIG 712	UGC 10083/NGC 6012	15 54 13.74	+14 36 06.9	1854	55	Sbc	(R_2)SA(r)b
KIG 716	UGC 10104	15 57 27.86	+30 03 34.6	9841	13	Sc	SA(rs)bc
KIG 719	UGC 10120	15 59 09.56	+35 01 47.2	9438	22	Sb	(R'_1)SB(r)b
KIG 731		16 17 39.45	+10 21 45.7	9817	46	Sb	SAB(rs)bc
KIG 743	UGC 10435	16 31 21.62	+22 41 49.3	7297	43	Sb	SB(rs)b
KIG 754	UGC 10490	16 38 49.56	+17 21 11.6	4594	45	Sc	SA(rs)b
KIG 757		16 39 30.75	+21 19 02.2	9338	48	Sbc	SAB(s)bc
KIG 795	UGC 10774	17 14 08.93	+58 49 06.3	8873	53	Sc	SAB(rs)bc
KIG 805	UGC 10829	17 23 47.31	+26 29 11.6	4730	51	Sbc	SA(rs)bc
KIG 807		17 23 09.59	+63 54 28.4	8228	57	Sbc	SA(s)bc
KIG 839		17 56 03.62	+49 01 41.7	9458	45	Sbc	SAB(s)c
KIG 892		20 52 22.38	+00 04 32.3	9087	36	Sc	SA(rs)bc
KIG 907		21 20 21.01	+10 19 13.6	5257	55	Sbc	SA(s)bc
KIG 912		21 23 22.14	+10 07 59.9	5122	53	Sb	SA(rs)c
KIG 924	UGC 11790	21 41 29.92	+00 53 40.8	4540	39	Sc	SA(s)bc
KIG 928		21 45 54.72	+11 40 41.5	6985	19	Sc	SA(s)bc
KIG 931	UGC 11816	21 49 07.30	+00 26 50.5	4750	0	Sbc	(R_2)SA(s)bc
KIG 932	UGC 11817/NGC 7138	21 49 01.10	+12 30 51.9	8406	59	Sbc	SB(r)b
KIG 943		22 04 12.67	−00 01 52.5	9778	46	Sb	(R'_1)SB(rs)b
KIG 250	UGC 04393	08 26 04.51	+45 58 06.0	2125	52	Sc	SB(s)dm
KIG 291	UGC 04684	08 56 40.68	+00 22 29.6	2521	23	Sc	SAB(rs)d
KIG 308		09 09 34.93	+18 36 56.9	8487	12	Sc	SA(s)ab
KIG 392		10 03 23.21	+48 21 56.6	7413	40	Sbc	SAB(r)ab

Column (1): KIG name. Column (2): UGC/NGC name. Column (3): right ascension (J2000). Column (4): declination (J2000). Column (5): recession velocity (km s^{-1}). Column (6): inclination in degrees. Column (7): morphological type – Sulentic et al. (2006). Column (8): morphological type – revised classification. The last four galaxies in this table (between horizontal lines) were excluded from our sample, because according to our revised classification they are not in the range Sb–Sc.
References – (i) Sulentic et al. (2006).

the isophote where the disc surface brightness profile drops to 25th mag arcsec^{-2}; (b) distribution of inclination; (c) distribution of i band absolute magnitudes M_i and (d) distribution of $(g - i)_o$ colour. The size a^i_{25} is calculated from the SDSS photometric parameter 'isoA'. The computation of $(g - i)_o$ is based on g- and i-band 'model' SDSS apparent magnitudes. The M_i is obtained from the SDSS i-band 'cmodel' magnitude (for more information on various types of galaxy magnitudes reported within SDSS, we direct the reader to: http://www.sdss.org/dr6/algorithms/photometry.html). We applied appropriate corrections to SDSS magnitudes and colours, i.e. Galactic and internal extinction, K-correction using YES[2] (York Extinction Solver; McCall 2004) and a $(1 + z)^4$ factor due to redshift dimming. The colour excess values $E(B - V)$ required as input for YES come from NASA Extragalactic Data base (NED)[3] are based on Schlegel, Finkbeiner & Davis (1998).

Each panel of Fig. 1 indicates the mean (± standard deviation) and the median for the distribution. The galaxies in our sample show semimajor axes covering a wide range between 4 and 28 kpc with the majority concentrated between 8 and 20 kpc (panel a). We visually examined galaxies in the first and last two bins of panel (a) (4–8 and 20–28 kpc). At the large end, we see galaxies with grand design spiral structure – luminosity class I (Sandage & Tammann

[2] http://cadwww.hia.nrc.ca/yes

[3] This research has made use of the NASA/IPAC Extragalactic Data base (NED) which is operated by the Jet Propulsion Laboratory, California Institute of Technology, under contract with the National Aeronautics and Space Administration.

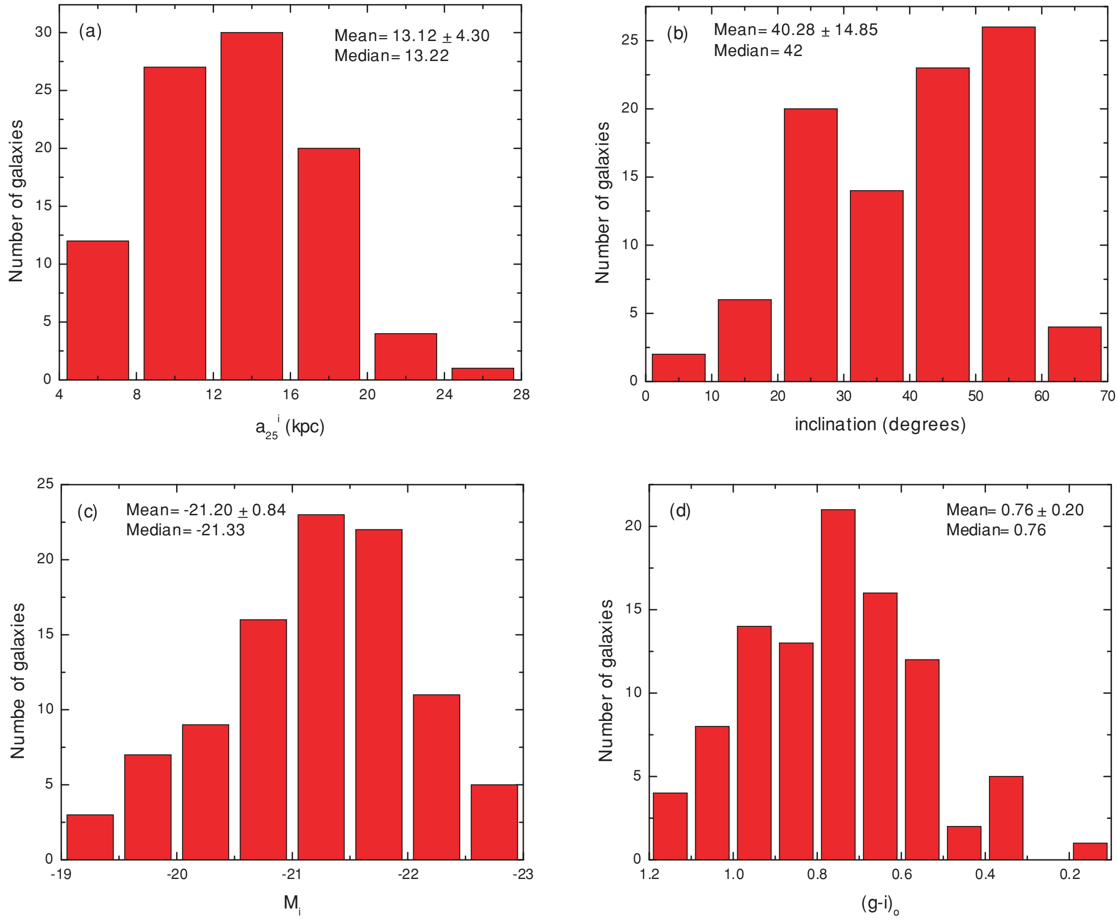

Figure 1. Basic properties of the Sb–Sc CIG sample: (a) the distribution of the disc size a^i_{25} in i band; (b) distribution of the inclination; (c) distribution of the total absolute magnitude M_i in i band; (d) distribution of the global colour $(g-i)_o$.

1981; van den Bergh 1960a,b). At the small end, we find a majority with flocculent structure characteristic of luminosity classes IV–V. One exception involves CIG522 which shows surprisingly grand design structure given its small size. Inclinations in our sample span a range from 0° to 70° with the bulk of the sample between 20° and 60° (panel b). Our sample covers a range in i band absolute magnitude from −19 to −23 (panel c), with an average absolute magnitude typical for an L^*-galaxy (e.g. Verdes-Montenegro et al. 2005). The faintest galaxies in our sample are similar in luminosity to the Large Magellanic Cloud (LMC). Galaxies in our sample show a wide spread in $(g-i)_o$ colours (0.1–1.2) with the bulk between 0.5 and 1 (panel d). Table 2 presents basic photometric measures based on SDSS photo-pipeline: $(g-i)_o$ colours, absolute global i-band magnitudes M_i and the a_{25} galactic semimajor axes both in i and g band. We checked our sample for biases driven by inclination effects and we found that SDSS photometric measures and BUDDA-derived parameters seem to be insensitive to inclination. Because our sample covers a wide range in redshift, it is affected by Malmquist bias. Lowest redshift favours the lowest luminosity galaxies and highest redshift the most luminous objects.

We also marked on all the plots in this paper (not shown in the paper) the galaxies classified in Sulentic et al. (2006) as I/A (interacting). The interaction code was either ‘y’ (KIG 446, 712) or ‘?’ (KIG 11, 33, 282, 328, 339, 366, 386, 466, 508, 640, 645, 743, 912, 943). A ‘y’ indicates a morphologically distorted system and/or almost certain interacting system while ‘?’ indicates evidence for interaction/asymmetry with/without certain detection of a companion. We find no trends for the galaxies flagged as I/A.

Table 3 presents average values (mean and median) for various interesting photometric measures, some of which having been employed in Fig. 2. Fig. 2(a) shows the correlation between disc size a^i_{25} and total i band absolute magnitude M_i. The three morphological types (Sb–Sbc–Sc) are shown with different symbols. The solid line represents the best-fitting linear regression[4] (correlation coefficient $R = 0.89$). Galaxies classified Sb and Sc favour opposite ends of the correlation with means (15.5 kpc; −21.5) and (12.2 kpc; −20.9), respectively. A similar correlation is seen when g band absolute magnitudes are used. Fig. 2(b) is a colour–magnitude diagram and indicates that the more luminous galaxies are also redder (e.g. Tully, Mould & Aaronson 1982; Wyse 1982; Gil de Paz et al. 2007), with linear regression correlation coefficient $R = 0.76$. Fig. 2(c) shows the relation between the galaxy colour $(g-i)_o$ and disc size a^i_{25} (linear regression correlation coefficient $R = 0.75$). We see that galaxies with larger discs tend to be redder than those with smaller discs. Correlations 2b and 2c appear to be largely driven by the location of Sb galaxies which tend to be larger, redder and more

[4] All correlation coefficients we report in this paper refer to an ordinary least-square linear regression of Y on X or OLS $(Y|X)$, e.g. Isobe et al. (1990). The errorbars of individual data points are not taken into account for linear regression fits.

Table 2. Photometric measures based on SDSS photo-pipeline.

Galaxy	$(g-i)_o$	M_i	a^i_{25} (kpc)	a^g_{25} (kpc)
KIG 11	0.61	−20.80	14.7	15.6
KIG 33	0.71	−21.50	13.8	13.1
KIG 56	0.99	−21.53	17.3	14.7
KIG 187	1.00	−22.18	19.5	17.3
KIG 198	1.15	−22.09	19.2	15.6
KIG 203	0.70	−21.09	13.9	12.0
KIG 217	0.85	−20.61	10.0	9.3
KIG 222	1.01	−21.40	13.3	11.4
KIG 232	1.09	−21.98	19.6	17.7
KIG 238	0.93	−21.30	17.2	13.0
KIG 241	0.52	−20.16	7.3	6.8
KIG 242	0.41	−19.36	5.9	5.7
KIG 258	0.76	−20.53	9.8	8.2
KIG 260	0.77	−21.57	18.7	17.7
KIG 271	0.79	−22.16	20.5	18.3
KIG 281	0.91	−21.32	15.5	14.3
KIG 282	0.93	−21.20	11.2	8.9
KIG 287	0.90	−21.79	16.8	16.0
KIG 292	0.72	−20.79	10.9	10.7
KIG 298	1.14	−22.55	18.4	17.9
KIG 302	0.87	−22.34	17.4	14.3
KIG 314	0.68	−21.60	16.3	14.5
KIG 325	0.82	−21.67	13.9	13.4
KIG 328	0.83	−21.53	13.6	12.2
KIG 330	0.66	−19.92	7.0	6.3
KIG 336	1.07	−22.21	18.9	17.4
KIG 339	0.94	−21.78	18.8	21.6
KIG 351	0.92	−20.74	12.7	11.5
KIG 365	0.73	−21.44	13.0	11.8
KIG 366	1.11	−21.88	16.2	14.4
KIG 367	0.69	−20.89	13.6	13.3
KIG 368	0.69	−21.90	16.0	15.2
KIG 386	0.82	−21.38	11.5	10.1
KIG 397	0.82	−20.53	8.5	5.9
KIG 399	0.77	−21.35	13.5	11.8
KIG 401	0.87	−21.57	15.4	14.3
KIG 405	0.73	−20.62	11.9	10.7
KIG 406	0.94	−21.61	15.4	11.6
KIG 409	0.52	−20.18	7.6	7.1
KIG 410	0.52	−21.01	10.1	9.2
KIG 429	0.88	−21.68	15.1	13.7
KIG 444	0.82	−21.29	8.5	7.7
KIG 446	0.80	−21.97	15.1	13.6
KIG 460	0.37	−20.12	7.9	8.5
KIG 466	0.50	−19.37	6.4	6.6
KIG 489	0.58	−21.07	10.8	10.4
KIG 491	0.85	−21.72	13.9	11.5
KIG 494	0.55	−20.74	10.3	10.4
KIG 499	0.94	−22.40	21.9	20.1
KIG 502	0.18	−19.24	11.2	11.0
KIG 508	0.56	−20.84	9.4	9.4
KIG 512	0.65	−19.70	9.6	9.0
KIG 515	0.68	−21.39	12.3	11.6
KIG 520	1.02	−22.20	17.7	16.7
KIG 522	0.56	−20.73	7.6	6.1
KIG 525	1.06	−22.01	20.8	18.0
KIG 532	0.59	−20.66	9.6	9.3
KIG 550	1.13	−22.97	26.2	23.6
KIG 553	0.88	−22.07	18.8	17.0
KIG 560	0.30	−20.08	7.0	6.6
KIG 571	0.65	−19.70	6.5	5.7
KIG 575	0.78	−20.77	9.7	9.0
KIG 580	0.63	−20.93	10.9	9.5
KIG 598	0.72	−22.18	13.5	12.7

Table 2 – *continued*

Galaxy	$(g-i)_o$	M_i	a^i_{25} (kpc)	a^g_{25} (kpc)
KIG 600	0.57	−19.94	8.4	8.3
KIG 612	1.05	−21.64	16.8	15.2
KIG 626	0.38	−20.53	11.9	11.3
KIG 630	0.76	−21.04	12.1	11.7
KIG 633	0.49	−20.02	5.1	4.5
KIG 639	0.63	−21.07	12.2	11.0
KIG 640	0.68	−21.13	9.2	7.1
KIG 641	1.03	−21.78	14.1	12.4
KIG 645	0.76	−20.44	8.9	8.5
KIG 652	0.67	−20.35	8.0	7.5
KIG 665	0.71	−21.03	11.9	11.0
KIG 671	0.92	−21.41	16.4	14.6
KIG 689	0.39	−19.90	8.5	7.1
KIG 712	0.58	−21.04	14.3	11.7
KIG 716	0.74	−23.00	44.1	31.7
KIG 719	0.79	−21.91	15.3	14.9
KIG 731	0.76	−21.41	13.2	12.4
KIG 743	0.94	−21.59	12.7	11.8
KIG 754	0.59	−19.98	9.6	8.5
KIG 757	0.69	−22.16	16.1	15.4
KIG 795	0.90	−21.85	15.7	15.1
KIG 805	0.83	−21.33	13.7	13.2
KIG 807	0.76	−21.54	12.3	10.5
KIG 839	0.75	−21.50	11.8	10.8
KIG 892	0.99	−22.59	17.1	14.7
KIG 907	0.40	−19.66	7.7	7.3
KIG 912	0.65	−20.40	8.2	8.0
KIG 924	0.76	−21.03	14.6	13.0
KIG 928	0.66	−20.30	6.6	5.5
KIG 931	0.88	−20.67	10.2	8.8
KIG 932	1.00	−22.81	22.0	19.4
KIG 943	0.70	−21.81	14.2	12.3

Column (1): galaxy name. Column (2): $(g-i)$ colour corrected for Galactic, internal extinction as well as *K*-corrected. Column (3): absolute magnitude in *i* band. Column (4): semimajor axis of $\mu_i = 25$ mag arcsec^{-2} isophote. Column (5): semimajor axis of $\mu_g = 25$ mag arcsec^{-2} isophote.

luminous than the other subclasses. Visual classification of Hubble subtypes, while rather subjective, appears to retain some utility for isolating galaxies according to first-order physical properties. All of the trends involving size, luminosity and colour are consistent with previous studies (e.g. Roberts & Haynes 1994; Shimasaku et al. 2001). Table 3 suggests that *i*-band a_{25} disc measures are systematically larger than corresponding *g*-band measures. This effect is likely caused by the lower signal-to-noise ratio (S/N) of the *g*-band images because the *i*-band filter is more sensitive[5].

The purpose of Figs 2(a)–(c) is two fold: to reveal correlations between basic properties and to identify outliers. The former correlations are expected to be better defined in a sample with minimal effects of nurture while, by the same reasoning, outliers are likely to indicate problematic data or remaining galaxies affected by interactions (that were not previously suspected as showing signs of interaction). The initial correlations based only on SDSS data revealed a small number of extreme outliers. We corrected all the measurements of the outlier galaxies (e.g. KIG: 397, 406, 502, 716 and 928). It became clear that the automated photometric SDSS pipeline cannot deal properly with galaxies that are strongly

[5] http://www.sdss.org/dr6/instruments/imager/index.html

Table 3. Mean/median for some photometric measures.

Type	M_i		$(g-i)_o$		a^i_{25} (kpc)		a^g_{25} (kpc)	
	Mean ± SE	median	Mean ± SE	median	Mean ± SE	median	Mean ± SE	median
Sb	−21.52 ± 0.14	−21.49	0.89 ± 0.03	0.92	15.5 ± 0.9	14.8	13.8 ± 0.8	12.7
Sbc	−21.25 ± 0.15	−21.38	0.76 ± 0.03	0.80	12.3 ± 0.7	13.5	11.2 ± 0.7	11.8
Sc	−20.92 ± 0.13	−20.91	0.67 ± 0.03	0.68	12.2 ± 0.7	11.8	11.1 ± 0.6	10.7
Sb-Sc	−21.20 ± 0.08	−21.33	0.76 ± 0.02	0.76	13.1 ± 0.4	13.2	11.9 ± 0.4	11.7

Note: *SE* is standard deviation of the mean.
Column (1): morphological type. Column (2): absolute magnitude in *i* band. Column (3): $(g-i)$ colour corrected for galactic, internal extinction as well as *K*-corrected. Column (4): semimajor axis of $\mu_i = 25$ mag arcsec^{-2} isophote. Column (5): semimajor axis of $\mu_g = 25$ mag arcsec^{-2} isophote.

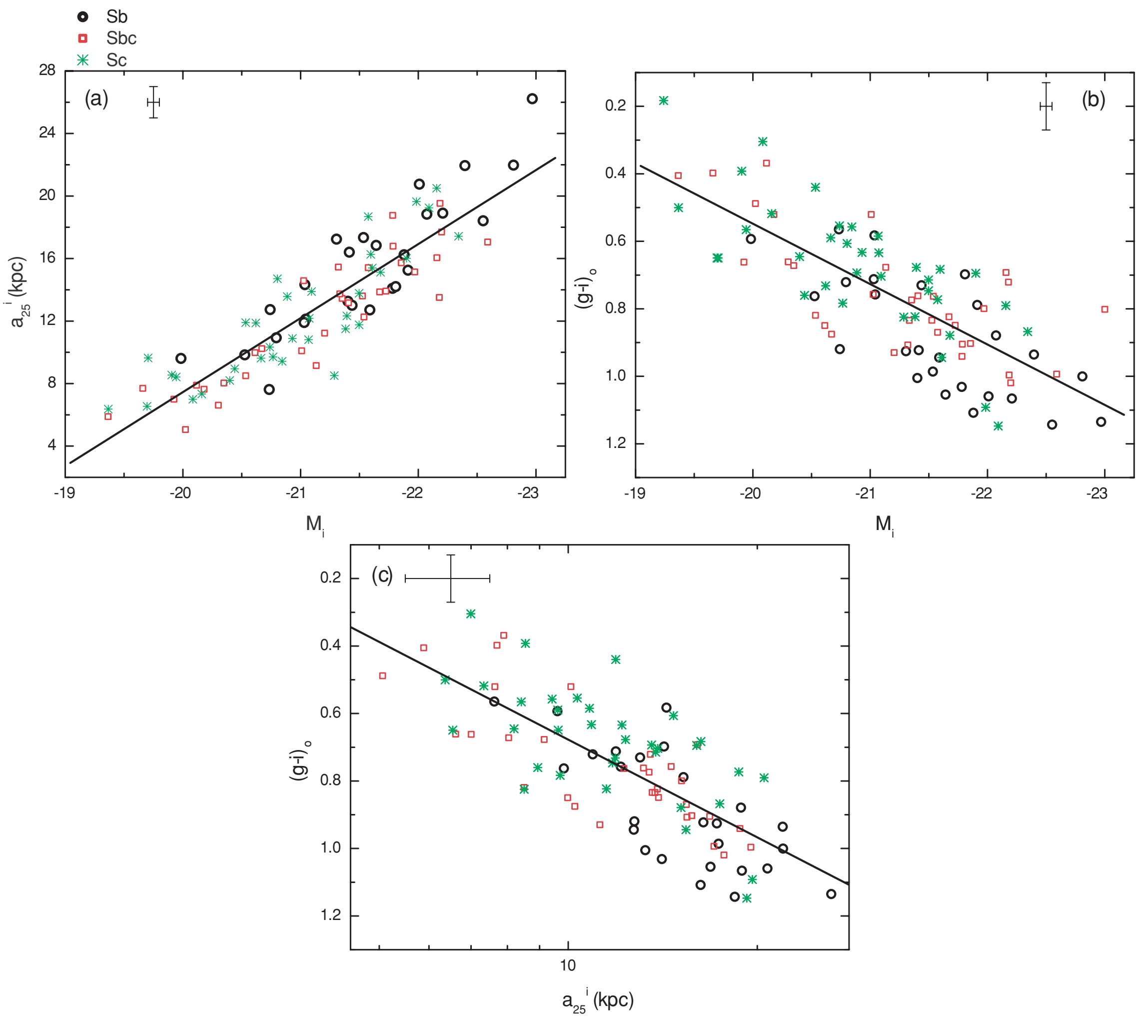

Figure 2. (a) Disc size a^i_{25} – absolute magnitude M_i diagram. (b) Colour $(g-i)_o$ versus total *i* band absolute magnitude M_i. (c) Colour $(g-i)_o$ versus disc size a^i_{25} in *i* band. The three morphological types (Sb–Sbc–Sc) are shown with different symbols. A linear regression fit to the whole sample is shown in each panel. The typical 2σ errorbars are shown in each panel.

contaminated by nearby bright stars. One galaxy (KIG 924) did not have any photometric measurements and two more galaxies (KIG 491 and 712) did not have any isoA measurements in the SDSS pipeline. For a few other galaxies, SDSS provided measures that fell away from the correlations well described by the rest of our sample. The SDSS magnitudes of the galaxies that fell on the correlations agree within 0.1–0.2 mag with our new measurements. Two galaxies (KIG 502 and KIG 716) show an a^i_{25} too large for their absolute magnitudes. These two galaxies show peripheral structures that raise the possibility they were affected by an interaction or accretion event. We conclude that the natural sizes of the galaxies KIG 502 and KIG 716 are much smaller than suggested by a^i_{25}. They are excluded from Figs 1(a), 2(a) and (c). One galaxy (KIG 322) was excluded from the sample because the contamination of the nearby bright star makes it impossible to obtain reliable photometric measurements.

We derive the following best-fitting regressions for the panels of Fig. 2: (a) $a^i_{25} = -87.27–4.74 * M_i$; (b) $(g - i)_o = -3.03 - 0.18 * M_i$ and (c) $(g - i)_o = -0.28 + 0.96 * \log (a^i_{25})$.

2.3 The choice of SDSS *i*-band images

The BUDDA-based decomposition and evaluation of CAS parameters reported in later sections are performed on SDSS *i*-band images. The choice of *i* band was motivated by several considerations: (i) the internal extinction in *i* band is significantly less than in a bluer filter, for example, is ∼60 per cent of that in *g* band and ∼80 per cent of that in *r* band (based on the sample of galaxies discussed here using YES extinction solver), (ii) the presence of star-forming regions within spiral arms would be associated with Hα emission, which is almost exclusively contained within the *r* filter for the range of V_R we consider here and (iii) the BUDDA code models the galaxy stellar background, including bars (best revealed by a redder filter) and does not fit the spiral structure (best traced by a bluer filter). The typical surface brightness zero-point for the *i*-band images we used is ∼26 mag arcsec^{-2}.

3 DATA REDUCTION

We used the *i*-band frames that are flat-field, bias, cosmic ray and pixel-defect corrected within the SDSS photometric pipeline (Stoughton et al. 2002). In a few cases more than one frame was needed in order to fully reconstruct the image of a galaxy. Frames were combined using IRAF[6] task IMCOMBINE. We cleaned images removing contaminating stars using the IRAF task IMEDIT. The sky was fitted with a 2D second-order polynomial and subtracted from the image using IRAF tasks IMSURFIT. Photometric calibration[7] was accomplished with *aa*, *kk* and *airmass* coefficients (zero-point, extinction coefficient and airmass) from the SDSS TsField files. We computed the zero-point for the surface brightness using $2.5 \times \log (exptime \times 0.396^2) - 2.5 \times 0.4 \times (aa + kk \times airmass)$, considering the exposure time *exptime* 53.907456 s and the pixel size 0.″396.

After performing these preliminary steps, we followed two different (but complementary) approaches towards describing quantitatively the galaxies structure and morphology.

(i) Bulge/disc/bar/AGN decomposition: We used BUDDA (de Souza et al. 2004) code version 2.1 to perform bulge/disc/bar/AGN decomposition. The program can fit simultaneously multiple components: a Sérsic bulge, two exponential discs, a Sérsic bar and a Moffat central source (active galactic nucleus – AGN).
The Sérsic surface brightness profile (Sérsic 1968) is described by

$$\mu(r) = \mu_e + c_n \left[(r/r_e)^{1/n} - 1\right],$$

where r_e is the effective radius (half-light radius), μ_e is the effective surface brightness (surface brightness at r_e), *n* is the Sérsic index – a parameter describing the shape of the profile and $c_n = 2.5(0.868n - 0.142)$. A Sérsic model is most suitable to describe the shape of luminosity profiles in bulges of galaxies (Andredakis, Peletier & Balcells 1995). A pure de Vaucouleurs profile (de Vaucouleurs 1948) is characterized by a Sérsic index of 4 and a pure exponential profile is described by a Sérsic index of 1. The Sérsic index $n_{\rm bulge}$ ranges from about 1 for late-type spiral galaxies (exponential profile, e.g. Andredakis & Sanders 1994; de Jong 1996) to about 6 for elliptical galaxies.

The exponential surface brightness profile of the disc (Freeman 1970) is given by

$$\mu(r) = \mu_o + 1.086 r/h_R,$$

where μ_o is the central surface brightness of the disc and h_R is the radial scalelength of the disc.

For a full description of the analytical functions used to fit each component see section 3.1 of Gadotti (2008). IRAF task ELLIPSE was used to get an initial guess for position angle (PA) and ellipticity (ϵ) for the bulge, disc and bar.

(ii) CAS parametrization: the concentration index appears to be an integral part of any morphological classification of galaxies (e.g. Bershady et al. 2000). The asymmetry and clumpiness indices are more sensitive to environmental (i.e. external) influences and are reasonable interaction diagnostics. Customarily, the three parameters are described quantitatively as follows.
Concentration $C = 5 \times \log (r_{80}/r_{20\rm percent})$, where r_{80} and $r_{20\rm percent}$ are the radii that include 80 and 20 per cent of the total light, respectively (cf. Conselice 2003).

Asymmetry $A_{abs} = \frac{\sum |I_0 - I_{180}|}{\sum |I_0|} - \frac{\sum |B_0 - B_{180}|}{\sum |I_0|}$, where I_0 and I_{180} represent the pixel light intensity in the initial and the 180° rotated image. The letter '*B*' in this context refers to the background and has a similar meaning. The summation is done over all pixels. The IRAF task IMCNTR identifies the centre of the galaxy (maximum intensity). The image is rotated 180° about that centre using the IRAF task ROTATE via linear interpolation. The standard procedure for computation of the asymmetry index involves also a minimization of *A* (see section 3.3 in Conselice et al. 2000). This method is effective for irregular and edge-on galaxies where the centroid is most uncertain. We note that Sb–Sc galaxies in our sample have a range of inclinations that allow less ambiguous determination of their centres, i.e. the brightest central grid point, whose coordinates are real numbers. In our cases, the uncertainty in identifying the centre of the galaxy using IMCNTR task is less than 1 per cent of a pixel. Therefore, we did not minimize the asymmetry index. None the less, we imposed the condition that the centre of the galaxy (initial estimate) does not shift upon rotation. We used IRAF task IMSHIFT to correct for any displacements that occurred.

Clumpiness $S = 10 \times [\frac{\sum (I_0 - I_\sigma)}{\sum I_0} - \frac{\sum (B_0 - B_\sigma)}{\sum I_0}]$, where I_0 and B_0 have the same meaning as in definition of A. The subscript 'σ' refers to the image that is smoothed with a boxcar of size $\sigma = 0.3 \times r(\eta = 0.2)$, where $r(\eta = 0.2)$ is the inverted Petrosian radius. We note that all central pixels (within 1/20 of the defined total radius of the galaxy) are set to nil value. Our *S*-definition is adapted from Taylor-Mager et al. (2007). We should also add that CAS is calculated within the total radius of the galaxy, defined as $1.5 \times r(\eta = 0.2).\eta(r) = \frac{I(r)}{\langle I(r) \rangle}$, where in practice $I(r)$ is the (mean) pixel-intensity at radius *r* from the Galactic Centre and $\langle I(r) \rangle$ is the average intensity within *r* (see also Takamiya 1999).

4 GALAXY DECOMPOSITION USING BUDDA

Fig. 3 shows examples of the BUDDA-based decomposition for the first four galaxies listed in Table 1 (ordered by CIG/KIG name). The left-hand panel displays, from left- to right-hand panel, the

[6] Image Reduction and Analysis Facility (IRAF) is distributed by the National Optical Astronomy Observatories, which are operated by the Association of Universities for Research in Astronomy, Inc., under cooperative agreement with the National Science Foundation – http://iraf.noao.edu/
[7] http://www.sdss.org/dr6/algorithms/fluxcal.html

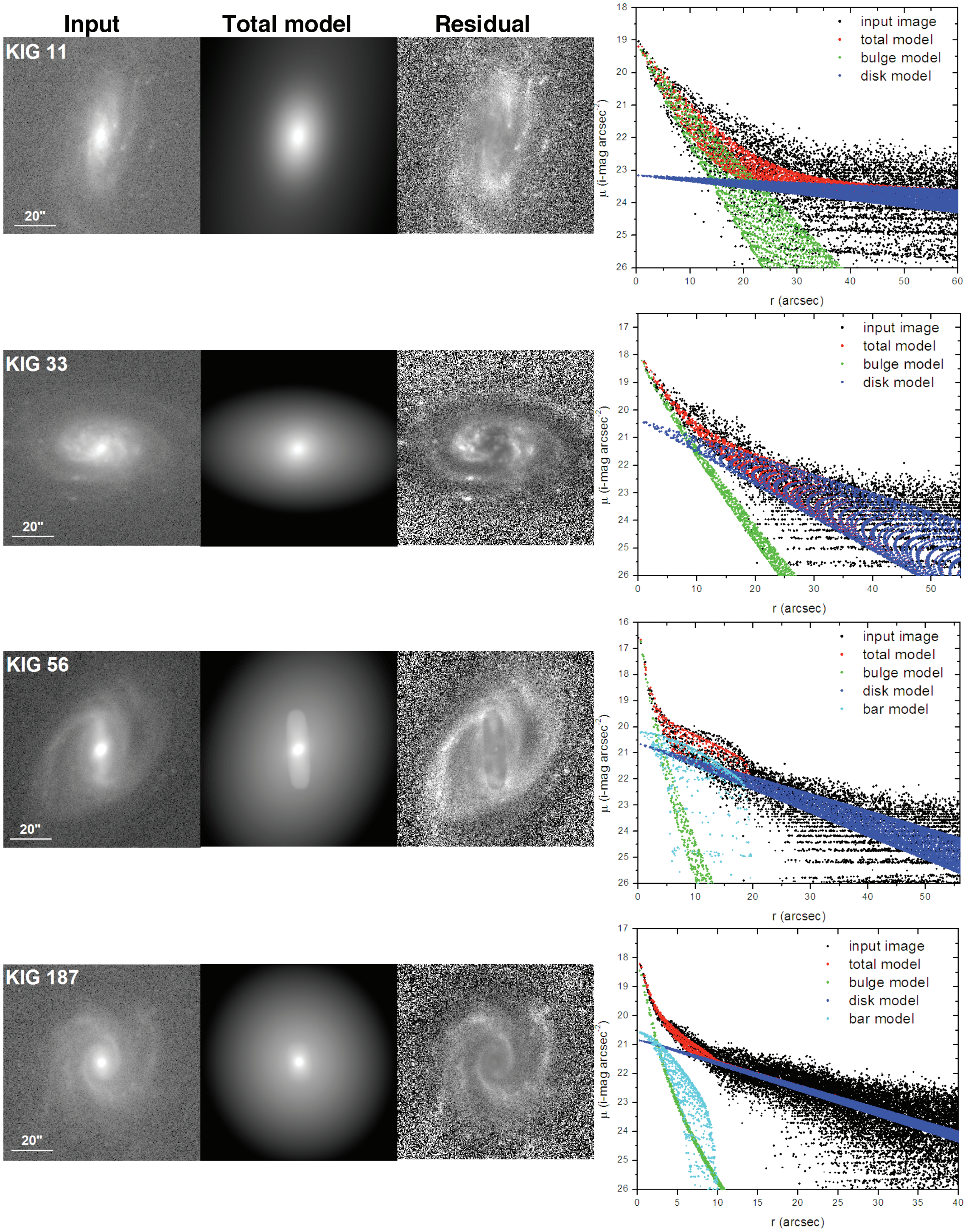

Figure 3. Examples of BUDDA-decomposition.

initial image, the fitted model and the enhanced residual image (initial image normalized by the model). The residual image shows high spatial frequency structure associated with the spiral arms and emission regions in each galaxy. The BUDDA code does not fit such high spatial frequency structure. The right-hand panel of Fig. 3 shows the surface brightness profile of the galaxy (black), fitted components (green = bulge, blue = disc and bar = turquoise) and total model (red; sum of all components). Data products for the entire sample are available at www.iaa.es/AMIGA.html. Table 4 provides a full set of parameters that describe the bulge–disc–bar components of the galaxies obtained using BUDDA[8]. We checked if our BUDDA parameters are affected by

[8] The surface brightness profiles shown in Fig. 3 and the numbers reported in columns (7) and (10) of Table 4 do not include Galactic extinction, $(1 + z)^4$ redshift dimming or K- corrections. However, everywhere else hereafter the averages (mean/median) are calculated after such corrections were applied. Moreover, all plots involving surface brightness μ_o and μ_e include the corrected values.

Table 4. Structural parameters obtained with BUDDA for CIG/KIG galaxies in our sample in *i* band.

(1) Galaxy	(2) Bulge/Total	(3) Disc/Total	(4) Bar/Total	(5) Bulge/Disc	(6) r_e (arcsec)	(7) μ_e ($\frac{mag}{arcsec^2}$)	(8) n_{bulge}	(9) h_R (arcsec)	(10) μ_o ($\frac{mag}{arcsec^2}$)	(11) l_{bar} (arcsec)	(12) n_{bar}
KIG 11	0.294	0.706		0.416	9.66	21.05	1.14	142.12	23.15		
KIG 33	0.349	0.651		0.536	5.71	20.04	1.17	16.08	20.33		
KIG 56	0.160	0.714	0.126	0.224	1.69	18.32	1.75	16.68	20.62	19.01	0.60
KIG 187	0.072	0.865	0.063	0.083	1.66	20.22	2.33	13.54	20.80	9.11	0.68
KIG 198	0.038	0.671	0.292	0.056	1.31	19.75	0.77	37.94	22.84	15.92	0.65
KIG 203	0.012	0.988		0.013	0.72	21.00	1.00	6.94	19.88		
KIG 217	0.040	0.960		0.042	2.09	20.54	2.55	15.77	20.36		
KIG 222	0.038	0.927	0.035	0.041	1.51	19.91	0.76	11.81	20.31	13.46	0.57
KIG 232	0.096	0.904		0.106	2.53	19.33	2.76	15.81	19.89		
KIG 238	0.150	0.688	0.163	0.217	1.48	19.44	1.97	19.87	22.19	11.88	0.59
KIG 241	0.010	0.990		0.010	1.04	20.92	0.37	5.18	19.66		
KIG 242	0.165	0.835		0.197	1.97	20.26	0.70	4.13	19.72		
KIG 258	0.204	0.766	0.030	0.267	1.32	19.66	2.90	8.26	20.55	8.71	1.05
KIG 260	0.020	0.949	0.031	0.021	1.84	21.08	1.93	14.92	20.77	9.90	0.60
KIG 271	0.020	0.964	0.016	0.020	1.36	20.85	2.09	11.45	20.01	7.92	0.62
KIG 281	0.024	0.976		0.024	1.80	20.04	1.07	15.86	20.04		
KIG 282	0.047	0.907	0.046	0.051	1.32	20.48	1.55	4.42	19.48	8.51	0.76
KIG 287	0.153	0.804	0.044	0.190	2.33	20.34	1.66	7.80	19.99	7.79	0.78
KIG 292	0.173	0.827		0.209	4.91	19.73	3.24	21.41	19.66		
KIG 298	0.123	0.805	0.071	0.153	2.04	18.81	1.78	19.38	20.52	19.80	0.70
KIG 302	0.103	0.897		0.115	1.93	19.78	1.03	6.33	19.05		
KIG 314	0.075	0.925		0.081	3.31	19.46	1.64	17.79	19.52		
KIG 325	0.083	0.917		0.091	1.78	20.07	1.10	8.69	20.15		
KIG 328	0.045	0.950	0.005	0.047	1.21	19.42	0.62	7.27	19.34	12.28	0.53
KIG 330	0.026	0.974		0.026	1.37	20.35	0.43	7.12	19.93		
KIG 336	0.213	0.662	0.125	0.322	2.87	19.47	2.09	26.79	21.79	22.18	0.50
KIG 339	0.299	0.564	0.137	0.531	2.37	18.92	2.60	54.07	22.91	21.78	0.48
KIG 351	0.031	0.867	0.102	0.036	1.16	20.11	0.34	11.83	20.97	11.09	0.53
KIG 365	0.051	0.898	0.051	0.057	1.11	19.52	0.90	7.81	20.37	10.30	0.76
KIG 366	0.081	0.779	0.140	0.104	1.50	19.44	1.90	9.53	19.70	16.24	0.82
KIG 367	0.216	0.784		0.276	7.08	22.04	1.55	58.30	23.19		
KIG 368	0.061	0.939		0.065	1.24	19.91	1.10	7.42	20.11		
KIG 386	0.025	0.962	0.014	0.026	0.84	19.75	0.66	5.73	19.24	6.53	0.47
KIG 397	0.060	0.930	0.010	0.064	1.92	19.61	1.56	7.65	18.76	5.94	0.60
KIG 399	0.042	0.958		0.044	1.50	20.14	1.46	9.25	19.83		
KIG 401	0.007	0.969	0.024	0.008	0.83	20.59	0.60	9.69	19.77	4.99	0.70
KIG 405	0.056	0.944		0.059	1.99	20.79	1.13	19.29	21.74		
KIG 406	0.209	0.791		0.263	3.41	21.25	1.08	7.53	20.47		
KIG 409	0.004	0.962	0.034	0.004	1.00	21.85	0.40	4.54	19.62	4.75	0.62
KIG 410	0.065	0.935		0.070	1.22	19.36	0.63	6.06	19.63		
KIG 429	0.014	0.982	0.004	0.014	1.07	21.14	0.73	7.81	20.04	4.95	0.58
KIG 444	0.024	0.961	0.015	0.025	1.57	19.82	1.23	6.23	18.52	10.10	0.65
KIG 446	0.064	0.936		0.069	1.16	19.64	0.84	5.10	18.83		
KIG 460	0.053	0.947		0.056	1.83	20.83	0.54	5.00	19.48		
KIG 466	0.243	0.726	0.032	0.334	8.54	21.64	0.66	29.30	22.07	14.14	0.77
KIG 489	0.017	0.983		0.017	1.19	20.20	0.48	7.25	19.35		
KIG 491	0.076	0.924		0.083	1.60	19.76	1.66	7.45	19.28		
KIG 494	0.040	0.916	0.044	0.044	2.07	21.35	0.69	7.28	20.25	6.66	0.50
KIG 499	0.045	0.840	0.115	0.054	0.99	19.61	2.10	12.81	20.23	7.07	0.69
KIG 502	0.085	0.915		0.093	8.98	21.87	1.45	337.49	23.34		
KIG 508	0.031	0.912	0.057	0.034	1.19	19.70	1.41	11.00	20.61	5.94	0.70
KIG 512	0.016	0.951	0.033	0.017	3.93	21.45	1.50	38.30	21.74	19.80	0.62
KIG 515	0.044	0.952	0.003	0.046	2.43	20.96	0.88	7.13	19.42	5.15	1.37
KIG 520	0.094	0.866	0.040	0.109	1.94	19.87	1.97	8.38	19.60	8.17	0.71
KIG 522	0.123	0.742	0.135	0.166	0.77	18.76	2.50	4.02	19.16	7.92	0.50
KIG 525	0.150	0.795	0.055	0.189	2.04	19.08	2.69	14.67	20.50	13.07	0.91
KIG 532	0.040	0.844	0.116	0.048	1.54	19.80	0.51	5.89	20.02	6.34	0.85
KIG 550	0.066	0.879	0.055	0.075	1.96	18.98	1.32	19.67	20.43	15.84	0.63
KIG 553	0.331	0.557	0.112	0.593	2.82	18.76	3.38	68.00	22.99	24.95	0.45
KIG 560	0.143	0.857		0.166	1.76	20.24	0.65	4.04	19.79		
KIG 571	0.031	0.969		0.032	2.53	21.50	1.22	9.06	19.41		

Table 4 – *continued*

(1) Galaxy	(2) $\frac{\text{Bulge}}{\text{Total}}$	(3) $\frac{\text{Disc}}{\text{Total}}$	(4) $\frac{\text{Bar}}{\text{Total}}$	(5) $\frac{\text{Bulge}}{\text{Disc}}$	(6) r_e (arcsec)	(7) μ_e $\left(\frac{\text{mag}}{\text{arcsec}^2}\right)$	(8) n_{bulge}	(9) h_R (arcsec)	(10) μ_o $\left(\frac{mag}{arcsec^2}\right)$	(11) l_{bar} (arcsec)	(12) n_{bar}
KIG 575	0.038	0.962		0.040	2.57	20.42	1.50	11.73	19.08		
KIG 580	0.052	0.948		0.055	1.13	20.36	1.45	5.71	19.42		
KIG 598	0.052	0.937	0.011	0.055	1.36	19.50	1.96	10.33	19.48	11.88	0.74
KIG 612	0.153	0.768	0.079	0.199	1.63	19.35	2.22	15.76	21.32	13.88	0.44
KIG 626	0.004	0.982	0.014	0.004	1.47	20.71	1.60	34.42	20.64	9.90	0.67
KIG 630	0.061	0.939		0.065	2.56	20.24	0.86	12.71	19.69		
KIG 633	0.052	0.948		0.055	1.03	19.31	0.39	3.41	18.48		
KIG 639	0.033	0.967		0.034	0.80	20.27	1.02	5.25	19.71		
KIG 640	0.099	0.901		0.110	0.93	19.24	0.97	2.14	18.05		
KIG 641	0.141	0.801	0.058	0.176	1.50	18.76	1.74	10.33	19.97	11.88	0.72
KIG 645	0.111	0.889		0.124	3.23	20.81	1.49	14.35	20.71		
KIG 652	0.029	0.940	0.031	0.031	1.17	19.03	1.84	12.09	19.39	8.32	1.19
KIG 665	0.086	0.914		0.094	1.90	20.56	0.98	6.73	19.70		
KIG 671	0.110	0.648	0.218	0.169	1.27	18.65	0.76	34.38	22.74	14.54	0.50
KIG 689	0.067	0.933		0.072	4.04	21.64	1.02	8.51	20.22		
KIG 712	0.059	0.941		0.062	5.06	20.72	1.05	22.06	19.65		
KIG 716	0.175	0.825		0.212	3.51	20.28	3.16	39.34	22.28		
KIG 719	0.121	0.679	0.153	0.186	1.27	18.84	1.28	14.88	21.42	14.26	0.63
KIG 731	0.040	0.885	0.075	0.045	0.81	19.91	0.94	5.96	20.16	7.92	0.31
KIG 743	0.056	0.865	0.079	0.064	1.32	20.23	2.11	14.10	21.10	13.46	0.30
KIG 757	0.074	0.847	0.079	0.088	1.16	19.48	2.24	7.29	19.61	11.29	0.79
KIG 795	0.046	0.954		0.048	1.45	20.61	1.53	9.12	19.99		
KIG 805	0.041	0.959		0.042	1.39	19.99	2.09	11.90	19.77		
KIG 807	0.022	0.978		0.023	1.02	20.03	0.70	5.07	19.01		
KIG 839	0.011	0.979	0.010	0.012	0.57	20.63	1.00	4.74	19.70	3.96	0.60
KIG 892	0.161	0.839		0.192	2.39	19.72	1.53	8.23	19.75		
KIG 907	0.303	0.697		0.435	4.93	21.49	0.87	71.95	23.46		
KIG 912	0.039	0.961		0.041	1.26	20.89	1.39	5.18	19.22		
KIG 924	0.018	0.982		0.018	1.63	20.63	0.60	17.81	20.95		
KIG 928	0.289	0.711		0.406	1.63	19.93	1.17	2.45	19.14		
KIG 931	0.120	0.880		0.137	5.12	21.33	1.75	16.36	21.29		
KIG 932	0.075	0.886	0.039	0.084	1.87	19.83	2.05	8.93	19.13	10.27	0.78
KIG 943	0.102	0.475	0.423	0.215	0.64	18.46	2.00	9.43	21.22	7.52	1.25

Column (1): galaxy name. Column (2): bulge/total luminosity ratio. Column (3): disc/total luminosity ratio. Column (4): bar/total luminosity ratio. Column (5): bulge/disc luminosity ratio. Column (6): effective radius of the bulge in arcsec. Column (7): effective surface brightness of the bulge in mag arcsec^{-2}. Column (8): Sérsic index of the bulge. Column (9): disc scalelength in arcsec. Column (10): central surface brightness of the disc in mag arcsec^{-2}. Column (11): bar length, i.e. semimajor axis of the bar in arcsec. Column (12): Sérsic index of the bar.

any biases and it turns out that the parameters derived by the code are insensitive to galaxy inclination and recession velocity. We conclude that the BUDDA code decomposition provides reasonable parametrization for all 94 galaxies. Two galaxies show clear shell structure (KIG 600 and KIG 754) suggesting that despite all of our efforts a few nurtured galaxies remain in the sample. The code was unable to model such complex structures, clearly overestimating the contribution of a bulge component (KIG 600) or not being able to isolate a bulge component at all (KIG 754). The sample consists of 25, 34 and 35 galaxies classified as Sb, Sbc and Sc, respectively, according to our reclassification using the SDSS images. We included an AGN component for two galaxies (KIG 671 and KIG 719) because they are classified as type 1 Seyfert in NED. All statistical analysis will be based upon results for the 94 galaxies suitable for BUDDA decomposition.

4.1 Properties of bulges

Spiral galaxies show a wide range of bulge sizes and bulge/disc luminosity ratios. It has been suggested that 'bulge building' via nurture processes (external acquisitions/accretion of companions) may be responsible for many or all large bulge systems (Carlberg 1999). Alternatively, other studies propose that dissipative processes in discs (internal secular evolution) are responsible for building up bulges in most spirals (e.g. Hunt, Pierini & Giovanardi 2004).

As expected, the fraction of CIG spirals with large bulges has decreased as classifications have evolved from the original low-resolution POSS to higher resolution POSS2 images and finally SDSS. If small bulge spirals represent some kind of primordial unnurtured spiral population then AMIGA/CIG represents the best sample to study the population statistically. It is especially interesting to quantify their properties in order to see how much of the known morphological and structural diversity is likely due to pure nature rather than nurture.

In the past 15–20 yr, the concept of exponential bulges has been systematically investigated and nowadays it is accepted that there exist two general types of bulges: classical and pseudo-bulges. A number of criteria (Kormendy & Kennicutt 2004) have been proposed to identify pseudo-bulges based upon: (i) morphological analysis of high-resolution Hubble images (they show flattened geometry, associated with nuclear spirals, rings or bars; e.g. Carollo 1999; Fisher & Drory 2008,), (ii) kinematics (they are described by low-velocity dispersion, which makes them outliers relative to the Faber–Jackson relation; Faber & Jackson 1976), (iii) photometric analysis of the surface brightness profile (they show nearly exponential profiles typical of discs[9]) and (iv) colour (age) of bulge stellar population (they may be dominated by Population I material, without obvious signs of mergers). In what follows, we evaluate the nature of bulges in our isolated sample by exploiting the photometric decomposition of the light profiles and we adopt a few simple criteria involving n_{bulge} and bulge/total luminosity ratio to distinguish between pseudo- from classical bulges.

It has been proposed that all galaxies with a bulge contribution (relative to the total galaxy luminosity) of 10 per cent or less are pseudo-bulges, i.e. disc-like structures formed by secular evolution (e.g. Kormendy & Kennicutt 2004; Laurikainen et al. 2007). About 68 per cent of our sample shows bulge/total ratios B/T < 0.1. Based on BUDDA parameters, ∼45 per cent of the Sb galaxies and 75–80 per cent of the Sbc–Sc galaxies show B/T < 0.1. A more extreme view (i.e. less restrictive) involves the proposal that all bulges characterized by $n_{bulge} < 2.5$ and B/T < 0.45 are pseudo-bulges (e.g. Kormendy & Kennicutt 2004; Drory & Fisher 2007). These considerations raise the possibility that ∼94 per cent of our sample contains pseudo-bulges. Applying similar criteria to the sample of $n = 95$ Sb–Sc galaxies from Laurikainen et al. (2004) [based on Ohio State University Bright Spiral Galaxy Survey (OSUBSGS) – Eskridge et al. 2002], we found a similar fraction ∼92 per cent pseudo-bulges. The latter sample was not selected using an isolation criterion, so a higher degree of nurtured galaxies might be expected. In this context, we note that a smaller fraction (59 per cent of the OSU sample) shows B/T < 0.1.

We note that the largest bulge/total ratio in our sample is B/T ∼ 0.35 and the largest n_{bulge} value we find is close to 3.5. The typical uncertainty in n_{bulge} is $\sigma \approx 0.5$ (confirming the result of Gadotti 2008). Fig. 4 shows the distribution of BUDDA-derived Sérsic bulge indices n_{bulge} versus the B/T ratio. The pseudo-bulge/classical bulge proposed boundaries mentioned above are indicated by dotted lines. Fig. 4 shows the strong concentration of much of our sample within the extreme pseudo-bulge domain. Although bulge/total is a rather robust empirical measure (Gadotti 2008), it is a very challenging task to quantify its uncertainties, which are not provided by the BUDDA code. We attempted to calculate the uncertainty of bulge/total varying the input parameters (giving BUDDA a range of reasonable starting values). We estimate (2–3σ) uncertainties generally smaller than 15 per cent.

In Fig. 4, the three morphological types Sb, Sbc and Sc are indicated with distinct symbols (see figure's legend). There are six galaxies (4 Sb and 2 Sbc) with $n_{bulge} > 2.5$ and bulge/total > 0.1 that could be interpreted as classical bulges because they lie outside the extreme suggested pseudo-bulge/classical bulge boundaries. 30 galaxies lie outside of the more restrictive pseudo-bulge domain with Sb again showing the largest fraction. This would still leave two-third of our sample (and most Sbc–Sc) as pseudo-bulge systems. The subset of Sb galaxies shows an apparent trend or a linear correlation in Fig. 4. Best-fitting regression line (solid) and

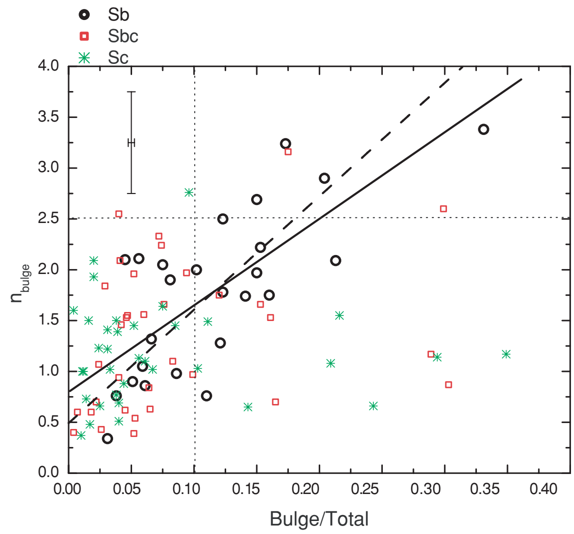

Figure 4. Bulge Sérsic index versus bulge/total luminosity ratio. A linear regression fit (solid line) and a bisector fit (dashed line) are shown for Sb-type only. The typical 2σ errorbars are shown.

bisector (dashed) are indicated for the Sb population. In either case, the correlation coefficient is $R \approx 0.7$. For the Sbc and Sc subsets, we find no evidence for a correlation (correlation coefficients $R \sim 0.3$–0.4 for Sbc types and 0.01–0.07 for Sc types). Clearly, the scatter increases with lateness of type. As a check for hidden luminosity trends in Fig. 4, we compared the location of the five least and most luminous galaxies (not shown here). Those points scatter everywhere on the plots suggesting no systematic effects on the distribution of measures.

Table 5 presents the average values (mean/median) of the structural parameters of bulges, discs and bars for the entire sample. The table is organized as follows. Column 1 – morphological type, column 2 – bulge/total luminosity ratio, column 3 – Sérsic index of the bulge n_{bulge}, column 4 – bulge effective radius r_e, column 5 – effective surface brightness of the bulge μ_e, column 6 – disc scalelength h_R, column 7 – central surface brightness of the disc μ_o. Table 5 shows a decreasing trend for a mean and median bulge/total and Sérsic index n_{bulge} measures from earlier to later types, with a larger gradient between Sb and Sbc than between Sbc and Sc. The Sérsic index n_{bulge} appears to be more sensitive to differences in Hubble type. We also point out that the bulge effective radius r_e shows no trend among Hubble subtypes (Table 5). Mean/median effective surface brightness increases from Sc to Sb by about 1.3 mag arcsec^{-2}.

Fig. 5(a) shows a 2D projection within the fundamental plane defined by μ_e (surface brightness at r_e) and r_e (Hamabe-Kormedy relation; Hamabe & Kormendy 1987) for bulges in our sample – (log r_e, μ_e) plane. The bulge effective surface brightness μ_e is corrected for Galactic extinction, $(1 + z)^4$ and K-corrected. There is no clear trend, as previously reported for late-type spiral bulges (Capaccioli, Caon & D'Onofrio 1992; Carollo 1999). We again see a separation between the earliest and latest types in our sample where Sb galaxies show the highest and Sc the lowest effective surface brightness (see also Table 5). The two outliers with lowest effective radii may be Sd galaxies. The segregation of morphological types is driven along the ordinate by lines of constant luminosity $L_T^{bulge} \propto I_e r_e^2$ in the (log r_e, μ_e) plane. Isolated Sb galaxies tend to be more luminous and have larger bulges compared to isolated Sc galaxies (see Tables 3

[9] It has been reported that dwarf elliptical galaxies also have Sérsic indices around 1 (see fig. 14 in Graham 2001b and fig. 11 in Graham & Worley 2008). This does not imply that such systems should be regarded as pseudobulges. Our following discussion pertains to spiral galaxies, i.e. galaxies that show bulges embedded in discs.

Table 5. Mean/median for structural parameters of bulges, discs and bars of all galaxies.

Type (*N*)	Bulge/Total		n_{bulge}		r_e (kpc)		μ_e		h_R (kpc)		μ_o	
	Mean ± SE	median	Mean ± SE	median	Mean ± SE	median	Mean ± SE	median	Mean ± SE	median	Mean ± SE	median
Sb (25)	0.12 ± 0.01	0.11	1.79 ± 0.17	1.90	0.73 ± 0.05	0.64	19.24 ± 0.13	19.30	7.40 ± 1.27	5.56	20.47 ± 0.21	20.34
Sbc (34)	0.09 ± 0.01	0.06	1.35 ± 0.13	1.32	0.74 ± 0.08	0.60	19.89 ± 0.12	19.85	5.23 ± 1.11	3.65	19.77 ± 0.19	19.52
Sc (35)	0.08 ± 0.01	0.04	1.18 ± 0.08	1.13	0.79 ± 0.10	0.65	20.48 ± 0.12	20.60	6.74 ± 1.58	3.59	20.21 ± 0.21	19.84
Sb-Sc (94)	0.09 ± 0.01	0.06	1.40 ± 0.07	1.30	0.76 ± 0.05	0.64	19.94 ± 0.09	19.90	6.37 ± 0.79	4.07	20.11 ± 0.12	19.80

Note: N = number of galaxies; *SE* is standard deviation of the mean.
Column (1): galaxy name. Column (2): bulge/total luminosity ratio. Column (3): Sérsic index of the bulge. Column (4): effective radius of the bulge in kpc. Column (5): effective surface brightness of the bulge in mag arcsec^{-2}. Column (6): disc scalelength in kpc. Column (7): central surface brightness of the disc in mag arcsec^{-2}.

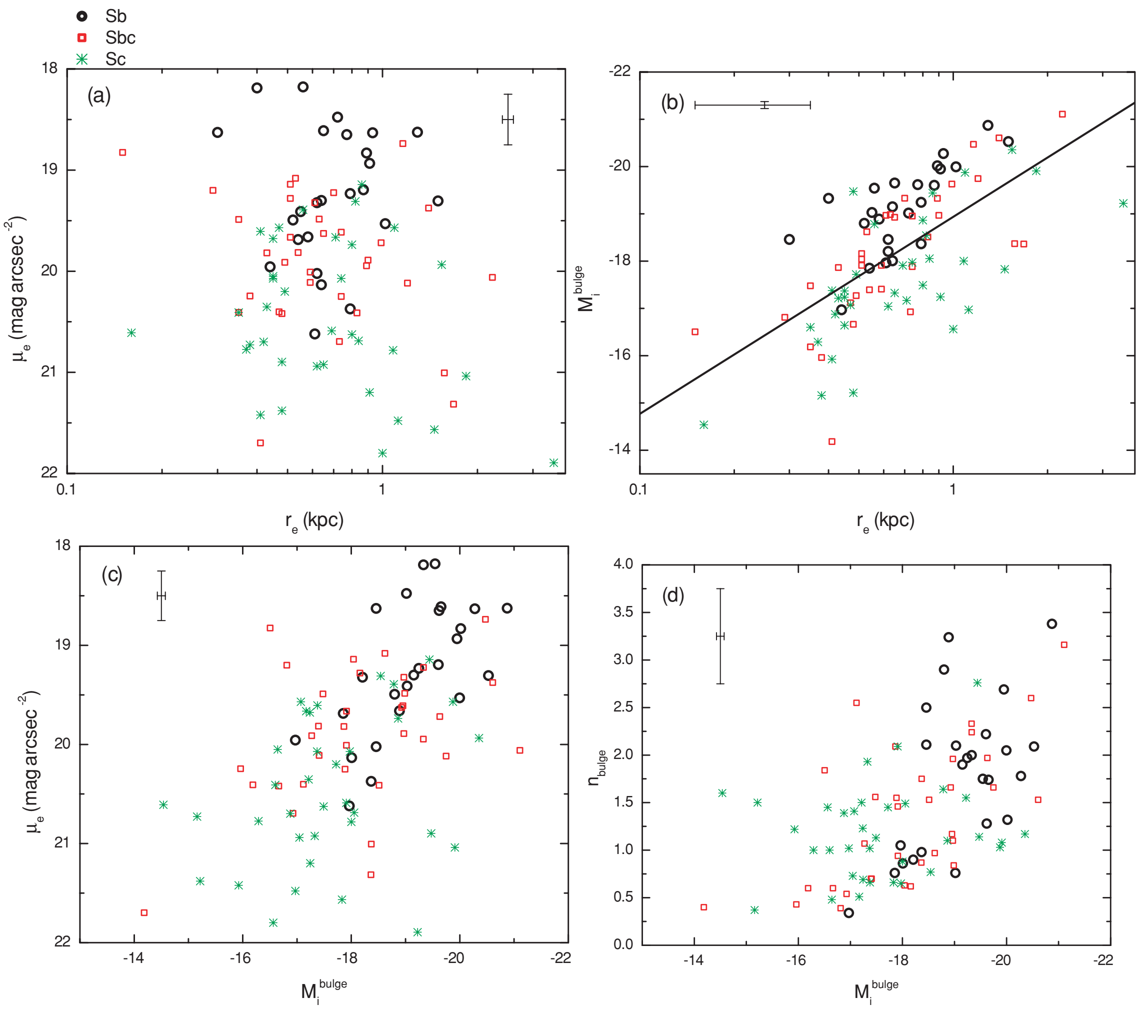

Figure 5. (a) Fundamental plane for bulges (effective surface brightness as a function of effective radius); (b–d) relationship between the parameters describing the bulge and its absolute *i*-band magnitude. The three morphological types are indicated with different symbols (see figure's legend). A linear regression fit to the whole sample is shown as a solid line (panel b). The typical 2σ errorbars are shown in each panel.

and 5). Galaxies with luminosities differing as much as 4 mag share the same range in r_e. Bulges in our Sb–Sc sample do not grow larger than $r_e \simeq 2.5$ kpc regardless of their luminosity. These results are consistent with those reported by Capaccioli et al. (1992) (see their fig. 4).

Fig. 5(b) shows the distribution of the bulge effective radius as a function of bulge absolute magnitude in *i* band, which can be regarded as a surrogate (log r_e, μ_e) plane. The M_i^{bulge} is obtained from the SDSS cmodel *i*-band magnitude of the galaxy (Section 2) taking into account the bulge/total luminosity ratio from the BUDDA code. The more luminous bulges show larger effective radii, although the correlation between the two parameters shows large scatter, with a linear regression correlation coefficient $R = 0.65$ (solid line). Actually, we see three parallel sequences of galaxies that we classify as Sb, Sbc and Sc, respectively. The r_e ranges are similar but Sc galaxies are displaced between $\Delta M_i = 1$–2 mag lower than Sb galaxies. Bulge effective radius is relatively insensitive to Hubble subtypes while bulge luminosity is useful in this context. This interpretation allows one to identify visually misclassified objects (or galaxies for which BUDDA-derived bulge parameters are unreliable).

Fig. 5(c) plots μ_e versus $M_i^{\rm bulge}$. It suggests that brighter bulges are also characterized by higher effective surface brightness, yet again the scatter is quite large. Fig. 5(d) displays the distribution of the bulge Sérsic indices as a function of $M_i^{\rm bulge}$. Fainter bulges tend to have lower values for $n_{\rm bulge}$.

4.2 Properties of bars

Visual inspection of SDSS *i*-band images suggests that 57 per cent of our sample (55 out of 96) could be classified as SB or SAB, showing bars or ovals. This fraction is consistent with that reported in other studies (in near-IR or *r* band) with no restriction on morphological type (Knapen 1999; Eskridge et al. 2000; Marinova & Jogee 2007; Menéndez-Delmestre et al. 2007; Verley et al. 2007c; Barazza, Jogee & Marinova 2008). The BUDDA code identified a bar component in 51 per cent of the sample (48 out of 94). There is a slight discrepancy between our visual estimate and BUDDA results (55 versus 48 barred galaxies, respectively). Six out of seven galaxies for which BUDDA did not identify a bar component were visually classified as SAB, i.e. transitional or intermediate between barred SB and non-barred SA. The most intriguing case is KIG 689, which visually could be classified as SB, yet the code cannot separate bulge-bar components.

We find that 34 galaxies have a bar/total luminosity ratio smaller than 10 per cent. The fraction of barred galaxies decreases from 84 (for Sb type) to ∼40–50 per cent for each of the later types Sbc and Sc. The BUDDA code provides a parameter called 'maximum radius of the bar', which we tabulate as $l_{\rm bar}$ and use as an estimate for the length of the bar (Gadotti 2008). Fig. 6 shows the distribution of $l_{\rm bar}$ (semimajor axis of the bar). Barred galaxies show a wide range $l_{\rm bar}$ = 1–12 kpc with a large concentration in the range ∼2–6 kpc.

Tables 6(a) and (b) present average values (mean/median) for the most important structural parameters for bulge, bar and disc components as estimated by BUDDA. We present numbers for barred (Table 6a) and non-barred (Table 6b) galaxies separately and by morphological subtype. Tables 6(a) and (b) are organized as

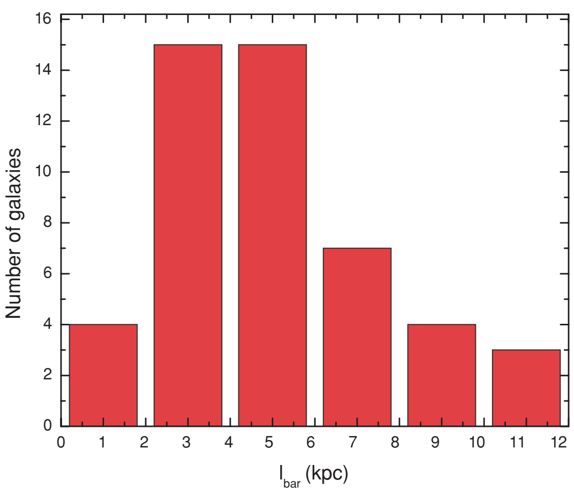

Figure 6. Bar size (semimajor axis of the bar) distribution for all barred Sb–Sc galaxies (N = 48).

Table 6a. Mean/median for structural parameters of bulges, discs and bars of barred galaxies.

Type (*N*)	Bulge/Total		$n_{\rm bulge}$		r_e (kpc)		μ_e		h_R (kpc)		μ_o		$l_{\rm bar}$ (kpc)	
	Mean ± SE	median	Mean ± SE	median	Mean ± SE	median	Mean ± SE	median	Mean ± SE	median	Mean ± SE	median	Mean ± SE	median
Sb (21)	0.12 ± 0.02	0.12	1.84 ± 0.16	1.97	0.74 ± 0.06	0.65	19.06 ± 0.12	19.19	8.29 ± 1.44	6.55	20.64 ± 0.23	20.38	6.48 ± 0.51	6.33
Sbc (13)	0.08 ± 0.02	0.05	1.56 ± 0.20	1.66	0.66 ± 0.09	0.61	19.75 ± 0.22	19.66	5.33 ± 1.81	4.03	19.72 ± 0.28	19.45	4.39 ± 0.72	4.79
Sc (14)	0.04 ± 0.02	0.02	1.12 ± 0.14	0.94	0.66 ± 0.09	0.64	20.45 ± 0.20	20.60	5.26 ± 1.44	4.00	20.25 ± 0.31	19.99	3.23 ± 0.55	2.90
Sb–Sc (48)	0.09 ± 0.01	0.05	1.55 ± 0.10	1.63	0.70 ± 0.04	0.65	19.65 ± 0.13	19.51	6.60 ± 0.91	4.54	20.28 ± 0.16	20.09	4.97 ± 0.39	4.78

Column (1): galaxy name. Column (2): bulge/total luminosity ratio. Column (3): Sérsic index of the bulge. Column (4): effective radius of the bulge in kpc. Column (5): effective surface brightness of the bulge in mag arcsec^{-2}. Column (6): disc scalelength in kpc. Column (7): central surface brightness of the disc in mag arcsec^{-2}. Column (8): bar length, i.e. semimajor axis of the bar in kpc.
Note: N = number of galaxies; *SE* is standard deviation of the mean; barred galaxies are those galaxies for which BUDDA returned a non-zero bar contribution.

Table 6b. Mean/median for structural parameters of bulges, discs and bars of non-barred galaxies.

Type (N)	Bulge/total		$n_{\rm bulge}$		$r_{\rm e}$ (kpc)		$\mu_{\rm e}$		$h_{\rm R}$ (kpc)		$\mu_{\rm o}$	
	mean ± SE	median	mean ± SE	median	mean ± SE	median	mean ± SE	median	mean ± SE	median	mean ± SE	median
Sb (4)	0.10 ± 0.03	0.07	1.53 ± 0.57	1.01	0.66 ± 0.05	0.63	20.20 ± 0.20	20.25	2.78 ± 0.14	2.72	19.56 ± 0.02	19.57
Sbc (21)	0.09 ± 0.02	0.06	1.23 ± 0.16	1.07	0.79 ± 0.11	0.59	19.98 ± 0.13	19.91	5.18 ± 1.45	3.57	19.80 ± 0.27	19.60
Sc (21)	0.10 ± 0.02	0.07	1.22 ± 0.10	1.14	0.88 ± 0.16	0.74	20.50 ± 0.16	20.63	7.74 ± 2.47	3.57	20.19 ± 0.30	19.65
Sb–Sc (46)	0.10 ± 0.01	0.06	1.25 ± 0.10	1.10	0.82 ± 0.09	0.62	20.24 ± 0.10	20.12	6.14 ± 1.31	3.09	19.96 ± 0.18	19.59

Note: N = number of galaxies; *SE* is standard deviation of the mean. Columns have the same designations like in Table 6(a).

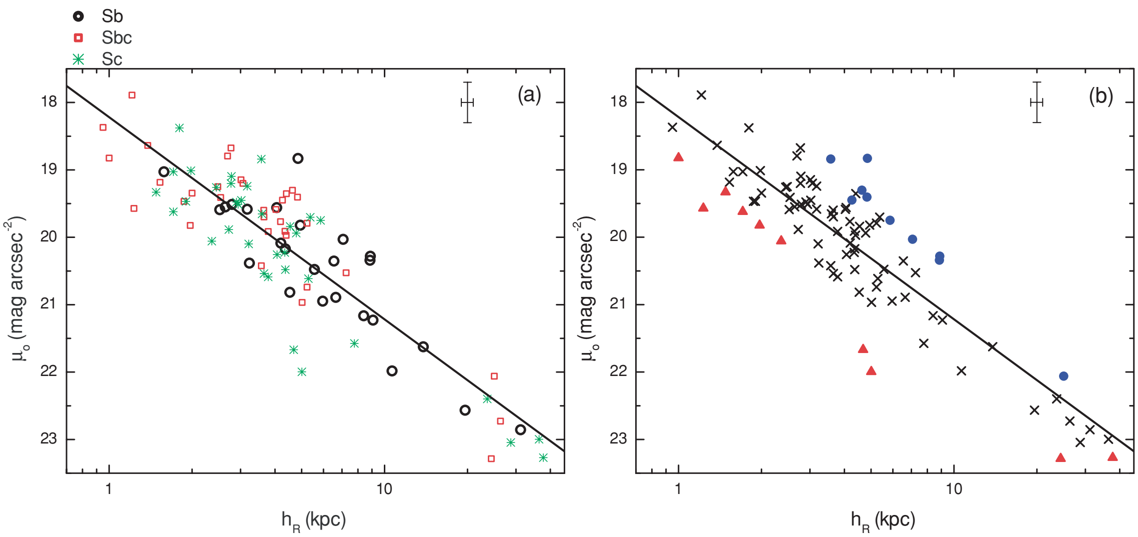

Figure 7. Relationship between the two parameters describing the disc profile, central surface brightness $\mu_{\rm o}$ versus disc scalelength $h_{\rm R}$. Panels (a) and (b) illustrate the same plot with the following differences: (a) the three morphological types are indicated with different symbols (see figure's legend). (b) Solid circles denote the 10 most luminous galaxies and solid triangles denote the 10 least luminous galaxies in our sample. In panel (b), we make no distinction between morphological types. A linear regression fit to the whole sample is shown as a solid line in both panels. The typical 2σ errorbars are shown in each panel.

follows: column 1 – morphological type, column 2 – bulge/total luminosity ratio, column 3 – $n_{\rm bulge}$, column 4 – bulge effective radius, column 5 – effective surface brightness of the bulge, column 6 – disc scalelength, column 7 – central surface brightness of the disc and column 8 – semimajor axis of the bar.

Table 6a indicates that $l_{\rm bar}$ decreases by a factor of 2 from Sb through Sc (qualitatively consistent with Erwin 2005; see also Combes & Elmegreen 1993; Zhang & Buta 2007).

4.3 Properties of discs

Fig. 7 illustrates the relation between the two parameters describing the disc exponential profile: $\mu_{\rm o}$ and h$_{\rm R}$. The surface brightness $\mu_{\rm o}$ was corrected for Galactic extinction. We also applied a $(1+z)^4$ and a K-correction. In Fig. 7(a), the three morphological types are indicated with different symbols Sb–Sbc–Sc. In Fig. 7(b), the 10 most luminous and the 10 least luminous galaxy discs in the sample are shown with solid circles and solid triangles, respectively. The 10 ten most luminous discs have absolute magnitudes in the range −22.8 to −22 and the 10 least luminous have absolute magnitudes in the range −19.9 to −19. The disc central surface brightness $\mu_{\rm o}$ and disc scalelength $h_{\rm R}$ are strongly correlated, with linear regression correlation coefficient $R = 0.88$ (see also Grosbøl 1985; Kent 1985; Khosroshahi, Wadadekar & Kembhavi 2000; Graham & de Blok 2001; Méndez-Abreu et al. 2008). The slope of the linear regression fit is 3.0 ± 0.2, well below a constant luminosity disc, which could be described by a slope of five (based on the approximation $L_T^{disc} \approx 2\pi I_{\rm o} h_{\rm R}^2$). This scaling relation seems to hold for all spiral types and it is observed for low surface brightness galaxies as well (Beijersbergen, de Blok & van der Hulst 1999). Other studies reported a slope in the range 1.5–3.0 (see Graham 2001a, and references therein). The ($\mu_{\rm o}$, log $h_{\rm R}$) plane is part of what some label as 'the fundamental plane' of spiral galaxy discs (e.g. Graham 2002; Shen, Mo & Shu 2002) described by $v_{\rm max}$, $\mu_{\rm o}$, $h_{\rm R}$, where $v_{\rm max}$ is the maximum rotation velocity. For a constant velocity, virial theorem expressed as $v_{\rm max}^2 \propto I_{\rm o}\, h_{\rm R}$ predicts a slope of 2.5, assuming a constant M/L (mass-to-light luminosity ratio). We find no morphological separation Sb–Sbc–Sc in the ($\mu_{\rm o}$, log $h_{\rm R}$) plane in our sample (Fig. 7a). A separation is seen when one compares more extreme morphological types (S0/Sa–Sb versus Scd–Sm/Irr; Graham & de Blok 2001). In Fig. 7(b), the 10 most luminous discs seem to define the upper envelope and the 10 least luminous the lower envelope of the $\mu_{\rm o}$–log $h_{\rm R}$ correlation. If we divide our sample in luminosity bins we would see parallel lines of constant luminosity in Fig. 7(b).

Most galaxies (∼90 per cent) have $h_{\rm R} < 10$ kpc. We observe that the Sb barred galaxies have a disc scalelength larger by a factor of 2 compared to the non-barred Sb galaxies. For Sbc and Sc galaxies, the presence/absence of bars does not appear to affect $h_{\rm R}$ (Tables 6a–b). We also note that the barred galaxies exhibit a significant change in the disc scalelength between Sb and Sbc–Sc (Table 6a), the earlier types Sb showing the largest values. In the case of non-barred galaxies, the trend is rather reversed (Table 6b).

Table 7. Mean/median for some photometric measures.

Type	a^i_{25}/h_R		l_{bar}/a^i_{25}		l_{bar}/h_R	
	Mean ± SE	median	Mean ± SE	median	Mean ± SE	median
Sb	2.9 ± 0.3	3.0	0.40 ± 0.03	0.37	0.98 ± 0.08	0.96
Sbc	3.9 ± 0.3	3.8	0.30 ± 0.04	0.26	1.06 ± 0.13	1.00
Sc	3.3 ± 0.2	3.6	0.26 ± 0.03	0.25	0.75 ± 0.09	0.68
Sb–Sc	3.4 ± 0.1	3.5	0.34 ± 0.02	0.34	0.93 ± 0.06	0.90

Note: *SE* is standard deviation of the mean.
Column (1): morphological type. Column (2): semimajor axis of μ_i = 25 mag arcsec^{-2} isophote normalized by the disc radial scalelength h_R. Column (3): semimajor axis of the bar normalized by the semimajor axis of μ_i = 25 mag arcsec^{-2} isophote. Column (4): semimajor axis of the bar normalized by disc radial scalelength h_R.

In Section 2, we found that the size of the disc decreases from Sb to Sc morphological type (Table 3). When a^i_{25} is normalized to the disc scalelength h_R, we get a rather different picture (Table 7). Sbc types are characterized by the largest values (also noted in Erwin 2005; see their Fig. 7).

4.4 Bar–bulge–disc scaling relations

4.4.1 Bar–bulge interplay

Fig. 8(a) shows n_{bulge} versus bulge/total luminosity ratio for the barred galaxies in the sample. Most barred galaxies with bulge/total > 0.1 are morphological type Sb (∼81 per cent); 67 per cent of all barred Sb–Sc fall in the high-probability pseudo-bulge space (bulge/total < 0.1). Sb galaxies show a correlation even when we restrict the plot only to barred galaxies. The correlation coefficients are $R \approx 0.7$ for both the regression line and the bisector fit, shown with a solid and a dashed line, respectively. Fig. 8(b) shows n_{bulge} versus bulge/total luminosity ratio for the non-barred galaxies in the sample; 70 per cent of all non-barred Sb–Sc fall in the high-probability pseudo-bulge space (bulge/total < 0.1). Non-barred galaxies appear to concentrate at lower values of n_{bulge} compared to the barred galaxies. One can note a scarce occupation for n_{bulge} > 1.7 for non-barred galaxies.

While for the barred galaxies, we see a tendency to get lower values for both bulge/total and the Sérsic index n_{bulge} from Sb to Sc, the non-barred galaxies show rather unchanged numbers (Tables 6a and b). We also point out that the bulge effective radius r_e does not appear sensitive to the presence/absence of bars (Tables 6a and b). While barred galaxies show lower effective surface brightness from Sb through Sc, non-barred galaxies do not appear to change in bulge effective surface brightness with morphological type (Tables 6a and b).

4.4.2 Bar–disc interplay

Fig. 9(a) shows a robust correlation between the size of the bar l_{bar} and the disc scalelength h_R, regression line correlation coefficient $R = 0.84$. Larger bars are hosted by larger discs. Fig. 9(b) suggests that larger bars are found in discs with lower central surface brightness μ_o. Fig. 9(c) indicates that the bar size is correlated with the absolute magnitude of the galaxy, linear regression correlation coefficient $R = 0.69$, the more luminous galaxies harboring the largest bars (Kormendy 1979).

Fig. 9(d) displays a relation between the galaxy colour $(g - i)_o$ and the size of the bar l_{bar}. We observe that larger bars are hosted by redder galaxies.

In panel (a), we presented a tight linear correlation between l_{bar} and the disc scalelength h_R. At this time, we would like to see if a similar correlation holds between bar length l_{bar} and the size of the disc a^i_{25} (Fig. 9e). Although a larger scatter is evident, the trend is consistent with the previously reported result (Fig. 9a), namely larger bars are hosted in larger discs.

As we reported in Section 4.2, the size of the bar l_{bar} appears dependent upon the morphological type, Sb hosting the largest bars and Sc the smallest ones. Even when l_{bar} is normalized to a^i_{25}, the trend is still preserved. However, if l_{bar} is normalized by h_R we note a similarity between Sb and Sbc galaxies and a rather large drop for Sc types (Table 7).

In all trends seen in Figs 9(a)–(e) one can note a morphological separation Sb–Sbc–Sc. At one end, Sb galaxies tend to have the largest bars, the largest discs, the lowest central surface brightness,

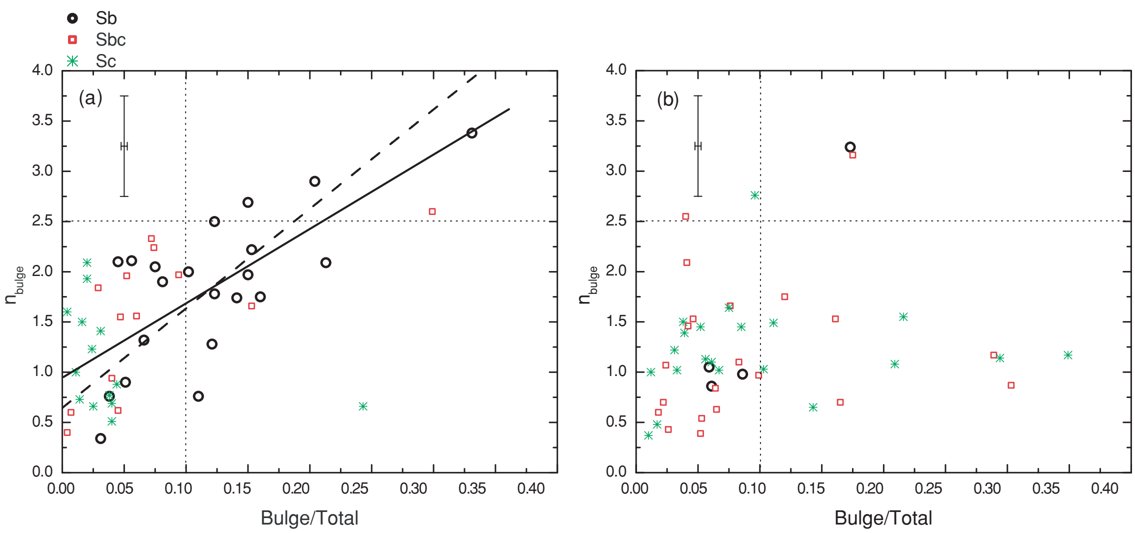

Figure 8. (a) Bulge Sérsic index versus bulge/total luminosity ratio for barred galaxies. (b) Bulge Sérsic index versus bulge/total luminosity ratio for non-barred galaxies. A linear regression fit (solid line) and a bisector fit (dashed line) are shown for only for Sb-type in panel (a). The three morphological types are indicated with different symbols (see figure's legend). The typical 2σ errorbars are shown in each panel.

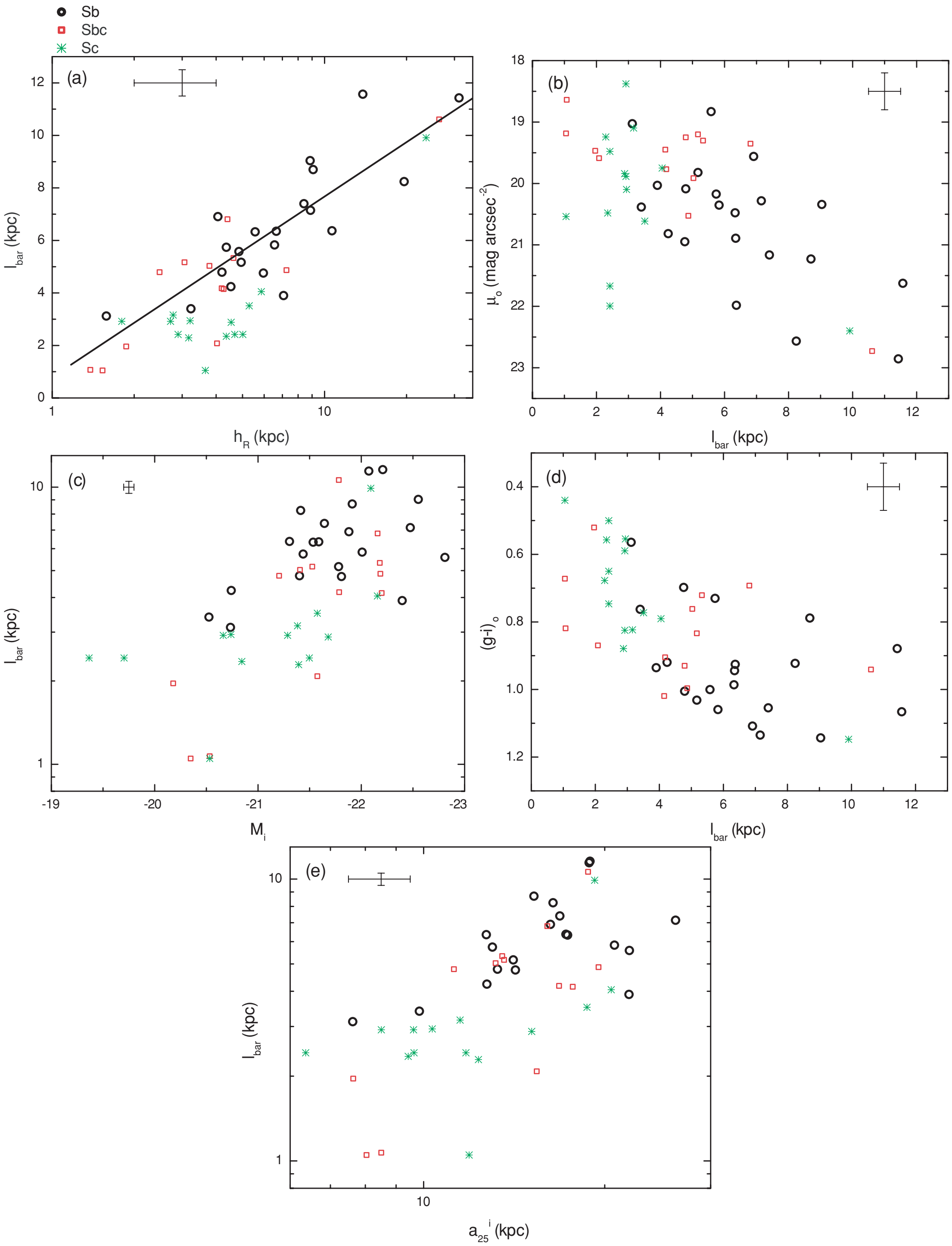

Figure 9. Relationship between bar size $l_{\rm bar}$ and the parameters describing the disc: disc scalelength $h_{\rm R}$ (panel a) and disc central surface brightness $\mu_{\rm o}$ (panel b). A linear regression fit for all barred galaxies in our sample (48) is shown as a solid line in panel (a). Panel (c) shows the relation between the size of the bar and the total absolute magnitude of the galaxy M_i. (d) Galaxy colour $(g-i)_{\rm o}$ versus bar size $l_{\rm bar}$. (e) Size of the bar $l_{\rm bar}$ versus the galaxy size a^i_{25}. The three morphological types are indicated with different symbols (see figure's legend). The typical 2σ errorbars are shown in each panel.

being the most luminous and the reddest. At the other end lie the Sc galaxies.

4.4.3 Bulge–disc interplay

Fig. 10(a) plots the bulge effective radius $r_{\rm e}$ versus the disc scalelength $h_{\rm R}$ (linear regression correlation coefficient $R = 0.55$). Larger bulges are associated with larger discs. Fig. 10(b) shows the bulge effective radius normalized to the disc scalelength as a function of bulge/total ratio. This later panel should be considered in conjunction with Tables 8(a) and (b). Table 8(a) presents the average values (mean/median) of $r_{\rm e}/h_{\rm R}$ for each morphological type (considering also barred versus non-barred galaxies) and Table 8(b) displays those averages for galaxies with bulge/total < 0.1 and bulge/total

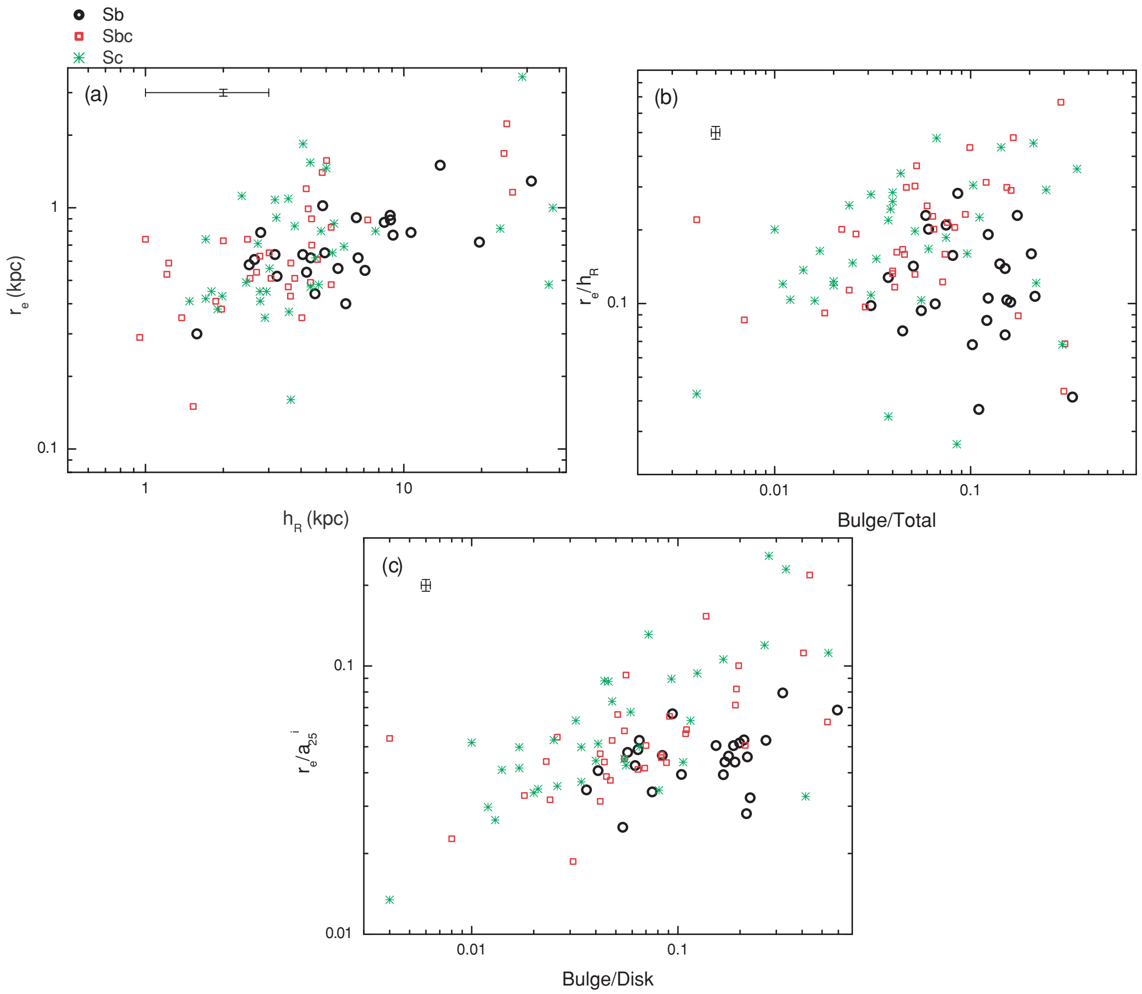

Figure 10. (a) Bulge effective radius r_e shown in relation to the scalelength of the disc h_R. (b) Bulge effective radius r_e normalized to disc scalelength h_R as a function of bulge/total luminosity ratio. (c) Bulge effective radius r_e normalized to the disc size a^i_{25} versus bulge/disc luminosity ratio. The three morphological types are indicated with different symbols (see figure's legend). The typical 2σ errorbars are shown in each panel.

Table 8a. Mean/median for r_e/h_R.

Type	All		Barred		Non-barred	
	Mean ± SE	median	Mean ± SE	median	Mean ± SE	median
Sb	0.13 ± 0.01	0.11	0.11 ± 0.01	0.10	0.24 ± 0.02	0.23
Sbc	0.22 ± 0.02	0.20	0.17 ± 0.02	0.16	0.24 ± 0.04	0.20
Sc	0.20 ± 0.02	0.17	0.17 ± 0.03	0.13	0.22 ± 0.03	0.20
Sb–Sc	0.19 ± 0.01	0.16	0.15 ± 0.01	0.13	0.23 ± 0.02	0.20

Note: *SE* is standard deviation of the mean.

> 0.1, respectively. We found a similar proportion (half–half) of barred/non-barred among galaxies with bulge/total < 0.1. The same relative distribution of barred/non-barred we find for galaxies with bulge/total > 0.1. We observe that non-barred galaxies have on average larger r_e/h_R than barred galaxies for all morphological types (Table 8a). This seems to be the case even when we divide the sample about bulge/total = 0.1 (Table 8b).

Three main conclusions emerge from Fig. 10b: (i) for galaxies with bulge/total < 0.1, the points appear evenly distributed about $r_e/h_R \sim 0.16$–0.18, (ii) the dispersion of r_e/h_R values increases as bulge/total gets larger and (iii) Sb galaxies seem to detach

Table 8b. Mean/median for r_e/h_R for bulge/total less than and larger than 0.1.

Type	Bulge/total < 0.1						Bulge/total > 0.1					
	All		Barred		Non-barred		All		Barred		Non-barred	
	Mean ± SE	median	Mean ± SE	median	Mean ± SE	median	Mean ± SE	median	Mean ± SE	median	Mean ± SE	median
Sb	0.16 ± 0.02	0.14	0.13 ± 0.02	0.11	0.24 ± 0.02	0.23	0.11 ± 0.02	0.10	0.10 ± 0.01	0.10		0.23
Sbc	0.19 ± 0.02	0.18	0.17 ± 0.02	0.16	0.21 ± 0.03	0.20	0.28 ± 0.08	0.29	0.17 ± 0.13	0.17	0.32 ± 0.01	0.30
Sc	0.18 ± 0.02	0.16	0.16 ± 0.03	0.12	0.19 ± 0.03	0.18	0.28 ± 0.05	0.30		0.29	0.28 ± 0.06	0.31
Sb–Sc	0.18 ± 0.01	0.16	0.16 ± 0.01	0.13	0.20 ± 0.02	0.20	0.20 ± 0.03	0.14	0.13 ± 0.02	0.10	0.29 ± 0.05	0.30

Note: *SE* is standard deviation of the mean.

themselves from a clear correlation described by Sbc and Sc galaxies (see also Laurikainen et al. 2007).

In Fig. 10(c), we test whether bulge/disc luminosity ratio scales with the bulge effective radius r_e normalized to the size of the disc a^i_{25}. The scatter is rather large, with an increasing dispersion for larger bulge/disc values. None the less, a global trend is evident, with r_e/a^i_{25} getting larger as bulge/disc gets larger. We see again, just like in panel (b), a separation of Sb galaxies from the rest of the sample, Sbc–Sc showing a correlation between the two parameters.

5 CAS PARAMETRIZATION – DATA ANALYSIS

CAS parameters are a useful diagnostic indicating possible interacting processes. Our sample is particularly useful in defining the natural levels of these parameters. We have considered for this part of the analysis our sample of $n = 96$ galaxies (including KIG 600 and KIG 754 for which we could not perform reliable BUDDA decomposition – see Section 4). The results are summarized in Table 9. Table 10 presents CAS averages (mean/median) measures. Concentration parameter C shows a clear decrement with morphological type from Sb to Sc. We also note that Sb galaxies appear more symmetric than Sbc–Sc types.

The three panels of Fig. 11 show the CS–CA–SA parameter planes for our isolated galaxies. The most significant correlation appears between the Clumpiness index S and the Concentration index C (linear regression correlation coefficient $R = 0.66$). The more concentrated galaxies appear clumpier as well. We note that Sb galaxies show a behaviour rather different relative to Sbc–Sc types. The former show a wide range of concentration indices (C) and are clustered in the region of very low values of asymmetry index (A), while the latter show a smaller extent in C, yet a much wider range of asymmetry.

6 COMBINING BUDDA-BASED AND CAS MEASURES

It is useful to look for trends between physical parameters that describe the larger scale (low-frequency) components of galaxies (i.e. BUDDA-based measures) and morphological parameters (i.e. CAS) that are sensitive to the higher frequency structures.

Figs 12(a)–(d) presents relationships between the Concentration index C and parameters that describe the bulge. As reported in previous sections, all measures (C, $n_{\rm bulge}$, bulge/total, μ_e) appear dependent upon the morphological type. Therefore, in general terms, the trends shown in the panels of Fig. 12 are somehow predictable. Yet, it is important to emphasize a few aspects: (i) for bulge/total < 0.1, galaxies show a clear linear correlation between bulge/total and C (linear regression correlation coefficient $R = 0.68$), but for bulge/total > 0.1 there is a large scatter in that plot (panels a and b); (ii) Concentration index C scales with the bulge Sérsic index $n_{\rm bulge}$ with an increasing dispersion as $n_{\rm bulge}$ gets larger (panel c); (iii) larger concentration indices C are found only in galaxies characterized by brighter bulge effective surface brightness μ_e (panel d) (see also Graham 2001b). We also find that more asymmetric galaxies (larger A) are restricted to brighter central surface brightness discs (μ_o) (Fig. 13). Barred and non-barred galaxies show very similar behaviour in the A–μ_o plane (not shown in the paper). The meaning of the curved trends illustrated in Figs 12(d) and 13 is not completely clear at this time. Extending the morphological range in both the directions outside the Sb–Sc morphological range may be relevant in this regard.

Table 9. CAS parameters.

Galaxy	C	A	S
KIG 11	3.39	0.05	0.27
KIG 33	3.04	0.12	0.22
KIG 56	4.18	0.07	0.26
KIG 187	3.22	0.04	0.20
KIG 198	3.19	0.08	0.21
KIG 203	2.63	0.02	0.20
KIG 217	2.52	0.08	0.15
KIG 222	2.57	0.06	0.15
KIG 232	3.06	0.28	0.23
KIG 238	4.25	0.07	0.28
KIG 241	2.44	0.11	0.15
KIG 242	3.19	0.05	0.20
KIG 258	3.77	0.12	0.19
KIG 260	2.86	0.11	0.22
KIG 271	2.71	0.08	0.18
KIG 281	2.42	0.05	0.14
KIG 282	2.95	0.17	0.23
KIG 287	3.53	0.07	0.30
KIG 292	3.18	0.08	0.19
KIG 298	3.69	0.07	0.22
KIG 302	2.89	0.26	0.17
KIG 314	3.22	0.09	0.26
KIG 325	2.94	0.08	0.21
KIG 328	2.61	0.11	0.16
KIG 330	2.45	0.13	0.15
KIG 336	3.96	0.04	0.24
KIG 339	5.70	0.04	0.29
KIG 351	2.79	0.05	0.21
KIG 365	2.58	0.14	0.16
KIG 366	3.45	0.05	0.26
KIG 367	3.10	0.06	0.22
KIG 368	2.79	0.10	0.21
KIG 386	2.56	0.18	0.20
KIG 397	2.83	0.19	0.21
KIG 399	2.68	0.13	0.20
KIG 401	2.61	0.03	0.16
KIG 405	2.51	0.03	0.15
KIG 406	2.61	0.10	0.14
KIG 409	2.47	0.11	0.17
KIG 410	2.76	0.28	0.20
KIG 429	2.41	0.06	0.16
KIG 444	2.62	0.28	0.15
KIG 446	2.82	0.07	0.25
KIG 460	2.96	0.07	0.18
KIG 466	3.01	0.23	0.12
KIG 489	2.65	0.17	0.18
KIG 491	2.95	0.07	0.26
KIG 494	2.82	0.16	0.20
KIG 499	3.70	0.05	0.22
KIG 502	3.71	0.01	0.27
KIG 508	2.88	0.19	0.17
KIG 512	2.47	0.00	0.16
KIG 515	2.84	0.08	0.22
KIG 520	3.34	0.07	0.24
KIG 522	3.06	0.04	0.14
KIG 525	3.88	0.08	0.24
KIG 532	3.04	0.18	0.18
KIG 550	3.14	0.07	0.19
KIG 553	4.90	0.03	0.34
KIG 560	3.20	0.09	0.25
KIG 571	2.70	0.10	0.19
KIG 575	3.00	0.08	0.25
KIG 580	2.79	0.08	0.16
KIG 598	2.80	0.12	0.18

Table 9 – *continued*

Galaxy	C	A	S
KIG 600	2.94	0.04	0.20
KIG 612	4.04	0.05	0.24
KIG 626	2.42	0.08	0.17
KIG 630	3.03	0.10	0.26
KIG 633	2.74	0.20	0.23
KIG 639	2.66	0.06	0.18
KIG 640	2.97	0.10	0.22
KIG 641	3.74	0.05	0.25
KIG 645	2.85	0.06	0.20
KIG 652	2.86	0.13	0.17
KIG 665	3.06	0.05	0.22
KIG 671	4.75	0.08	0.29
KIG 689	2.66	0.14	0.14
KIG 712	2.99	0.07	0.23
KIG 716	3.90	0.03	0.22
KIG 719	5.07	0.06	0.17
KIG 731	2.89	0.06	0.21
KIG 743	2.72	0.05	0.15
KIG 754	2.46	0.02	0.15
KIG 757	3.13	0.13	0.23
KIG 795	2.57	0.19	0.15
KIG 805	2.89	0.06	0.21
KIG 807	2.50	0.15	0.16
KIG 839	2.55	0.07	0.19
KIG 892	3.21	0.10	0.23
KIG 907	2.84	0.04	0.19
KIG 912	2.72	0.07	0.20
KIG 924	2.31	0.04	0.15
KIG 928	2.83	0.11	0.21
KIG 931	2.70	0.02	0.18
KIG 932	3.39	0.04	0.26
KIG 943	3.86	0.09	0.18

C – concentration. A – asymmetry. S – clumpiness.

Table 10. Mean/median for CAS parameters of all galaxies.

Type	C		A		S	
	Mean ± SE	median	Mean ± SE	median	Mean ± SE	median
Sb	3.55 ± 0.14	3.57	0.07 ± 0.01	0.06	0.22 ± 0.01	0.22
Sbc	2.94 ± 0.10	2.84	0.10 ± 0.01	0.08	0.20 ± 0.01	0.20
Sc	2.83 ± 0.05	2.80	0.11 ± 0.01	0.09	0.19 ± 0.01	0.19
Sb–Sc	3.06 ± 0.06	2.89	0.09 ± 0.01	0.08	0.20 ± 0.01	0.20

Note: *SE* is standard deviation of the mean.
Column (1): morphological type. Column (2): C – concentration. Column (3): A – asymmetry. Column (4): S – clumpiness.

7 DISCUSSION AND CONCLUSIONS

We have presented a detailed structural analysis for a well-defined sample of ∼100 late-type isolated galaxies. If a *bona fide* isolated (pure 'nature') population of galaxies exists then our previous work (Sulentic et al. 2006) suggests that it is dominated by systems with spiral morphology (∼84 per cent) with the bulk in the range Sb–Sc (63 per cent). We assume that the galaxies we investigate here are best described as 'minimal nurture and maximal nature' systems because they are as isolated as individual galaxies can be. This hypothesis does not imply that these isolated galaxies have undergone no merger activity since their epoch of formation but rather that major mergers are probably absent from their past ∼3 Gyr history. We do note that the AMIGA sample includes 14 per cent early-type galaxies and those are systems of such low luminosity as to suspect a little or no major merger activity over their entire history (Sulentic et al. 2006).

One might reasonably expect the tightest correlations between various intrinsic properties from a sample of isolated galaxies, where it is assumed that nurture (i.e. interactions) would increase the scatter (e.g. *UBV* colours; Larson & Tinsley 1978). The strength of this study is manifold: the large size of the sample, the uniformity of the SDSS data, the robustness of the BUDDA code and the stringent isolation criteria underlying the definition of the parent AMIGA sample. In this study, we have retained subjective morphological classifications and investigate morphological type dependence of various properties even though the typical range is narrow. This narrowness coupled with our 'nurture-free' assumption raises the possibility that Hubble type $T = 4 \pm 1$ may represent the seed population for all spiral galaxies.

7.1 Pseudo-bulges in isolated galaxies

We present evidence favouring the hypothesis that most or all late-type isolated galaxies host pseudo-bulges (Section 4.1) rather than classical bulges.

(i) A large majority of our isolated systems host relatively 'unevolved' bulge structures (as hypothesized by Hunt et al. 2004); most Sérsic indices ($n_{\rm bulge}$) are smaller than 2.0–2.5 (see Table 5 and Fig. 4) with the largest concentration around $n_{\rm bulge} \sim 1.3$–1.4. Such bulges are probably not as relaxed as larger bulges in earlier spiral types. They are likely dominated by rotation unlike higher Sérsic index bulges (for a detailed discussion on this subject see section 4.6 in Kormendy & Kennicutt 2004, section 4.2 in Laurikainen et al. 2007, and references therein).

(ii) We observe a large range of effective surface brightness $\mu_{\rm e}$ for a rather narrow range of $r_{\rm e}$ (these two last parameters defining in part the fundamental plane) – see Fig. 5a. The locus occupied by the bulges of our Sb–Sc galaxies in this plane is similar to that of disky bulges of galaxies at the end of dissipative collapse (Capaccioli et al. 1992). The lack of correlation between $\mu_{\rm e}$ and $r_{\rm e}$ supports the case of 'pseudo-bulges' for isolated spiral galaxies in our sample. As pointed out in MacArthur, Courteau & Holtzman (2003), these results support an 'iceberg' scenario, i.e. late-type spiral bulges are 'more deeply embedded in their host galaxy disc than earlier type bulges'. This idea is further complemented by the fact that the size of the bulge ($r_{\rm e}$) scales with the scalelength of the disc (Fig. 10a) (see also e.g. Khosroshahi et al. 2000; MacArthur et al. 2003; Fisher & Drory 2008; Méndez-Abreu et al. 2008).

We observe a larger dispersion in $r_{\rm e}/h_{\rm R}$ for larger bulge/total luminosity ratios (Fig. 10b). However, in Figs 10(b)–(c), one can clearly see that Sbc–Sc galaxies do show a clear increasing trend for $r_{\rm e}/h_{\rm R}$ and $r_{\rm e}/a^{i}_{25}$ with bulge/total and bulge/disc luminosity ratio, respectively. In contrast, Sb galaxies appear detached from the Sbc–Sc population. Assuming that the bulge Sérsic index and/or bulge/total luminosity ratios are reasonable discriminators of pseudo-bulges versus classical bulges (Section 4.1), then amongst our sample Sb galaxies have the greatest chance of hosting classical bulges. Thus, in Figs 10(b)–(c) we may have yet another indication that the pseudo-bulges and the galactic discs are clearly connected, while the classical bulges do not show similar scaling relations.

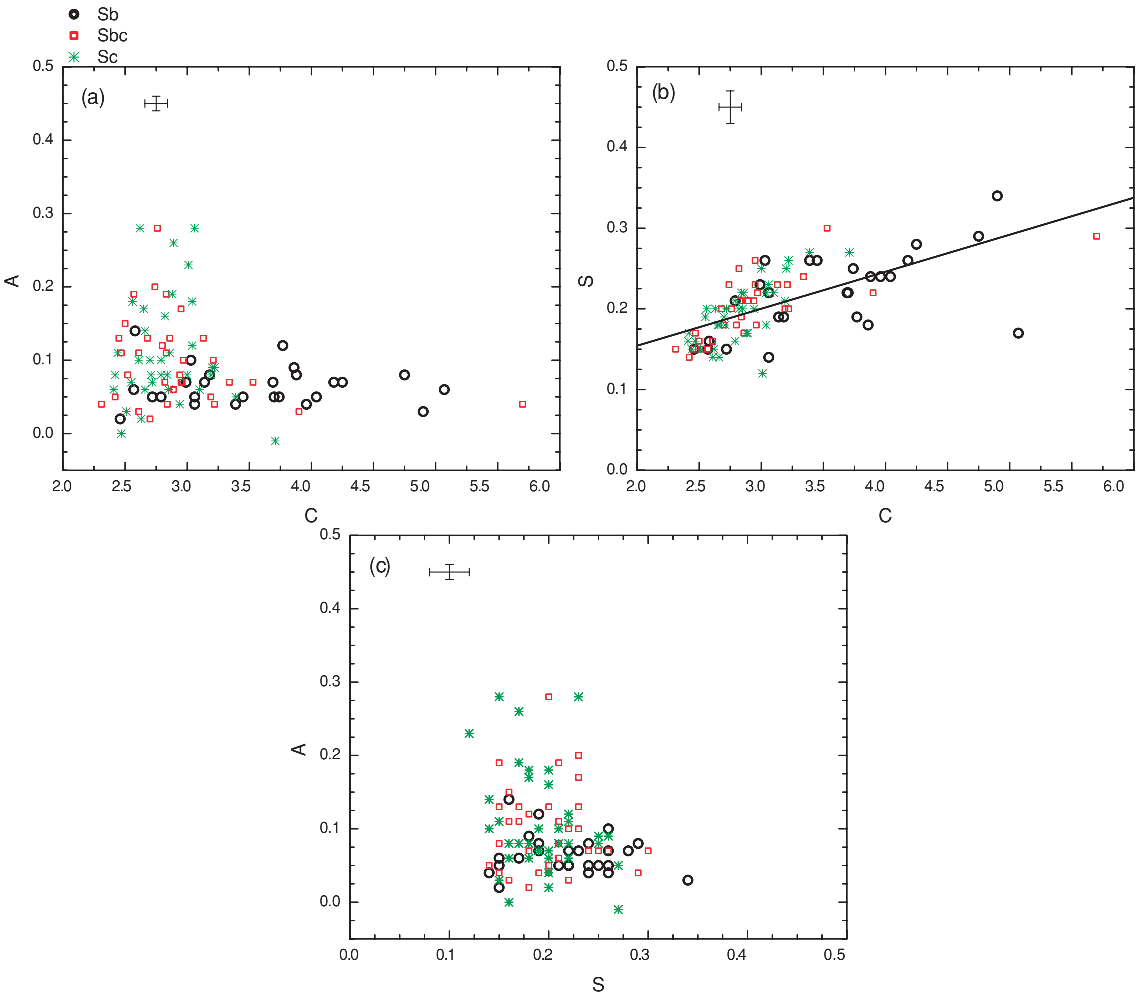

Figure 11. CAS parameters paired in AC–SC–AS planes in (a), (b) and (c), respectively. The three morphological types are indicated with different symbols (see figure's legend). A linear regression fit for the whole sample is shown as a solid line in panel (b). The typical 2σ errorbars are shown in each panel.

Some studies (e.g. Thomas & Davies 2006) argue that 'secular evolution through the disc and the phenomenon of pseudo-bulge formation are most likely restricted to spirals of types Sc and later'. Our results (but see also Laurikainen et al. 2007) find a large fraction of pseudo-bulges among spiral types earlier than Sc (see Section 4.1). This may be telling us that the formation of pseudo-bulges does not appear exclusively restricted to Sc types or later. Our results suggest that if one considers only morphological types later than Sc, one may identify an almost pure pseudo-bulge population of galaxies. A fundamental question mentioned earlier is whether the isolated Sb–Sc spiral galaxies constitute the seed population of unnurtured spirals? If so then isolated galaxies might be expected to host a pure pseudo-bulge population. In this context, Sb types in our sample have the greatest chance of bulge building via nurture and may involve a mixed classical and psuedo-bulge population. In Fig. 4, it is interesting that a linear correlation emerges only for galaxies of Sb type which bridges the classical and pseudo-bulges domains. Alternatively, the trend may be telling us that all/most Sb galaxies contain a real (classical) bulge. This would suggest that some large bulges are natural or that all Sb spirals in the sample are a product of nurture. The latter interpretation is disfavoured by the extreme isolation of our sample.

7.2 The role of bars in the formation of pseudo-bulges

The results of this study could set constraints for various galaxy formation and evolution models. Two important galaxy formation scenarios have been proposed and advocated: (i) spheroidal component (bulge) forms prior to the disc component in a monolithic collapse or via early mergers (so called 'inside out' formation, e.g. Eggen, Lynden-Bell & Sandage 1962; Baugh, Cole & Frenk 1996; Kauffmann 1996; van den Bosch 1998; Cole et al. 2000; Merlin & Chiosi 2006) and (ii) bulges form after the disc component as a result of secular dynamics/evolution driven by a disc instability (e.g. Courteau, de Jong & Broeils 1996; Zhang 2004) possibly triggered by external satellite accretion (e.g. Aguerri, Balcells & Peletier 2001; Eliche-Moral et al. 2006). The former mechanism may be dominant for elliptical galaxies and in early spiral galaxies with large bulges (as they all appear to share similar properties and scaling relations within the fundamental plane; e.g. Kormendy 1985; Djorgovski & Davis 1987; Faber et al. 1987). The latter mechanism may be more plausible for late-type spiral systems (e.g. Carollo 1999; Debattista et al. 2004; Hunt et al. 2004), as they largely harbor pseudo-bulges.

Some authors proposed that bulges of late-type spiral galaxies are formed primarily through secular evolution of bars (e.g. Kormendy

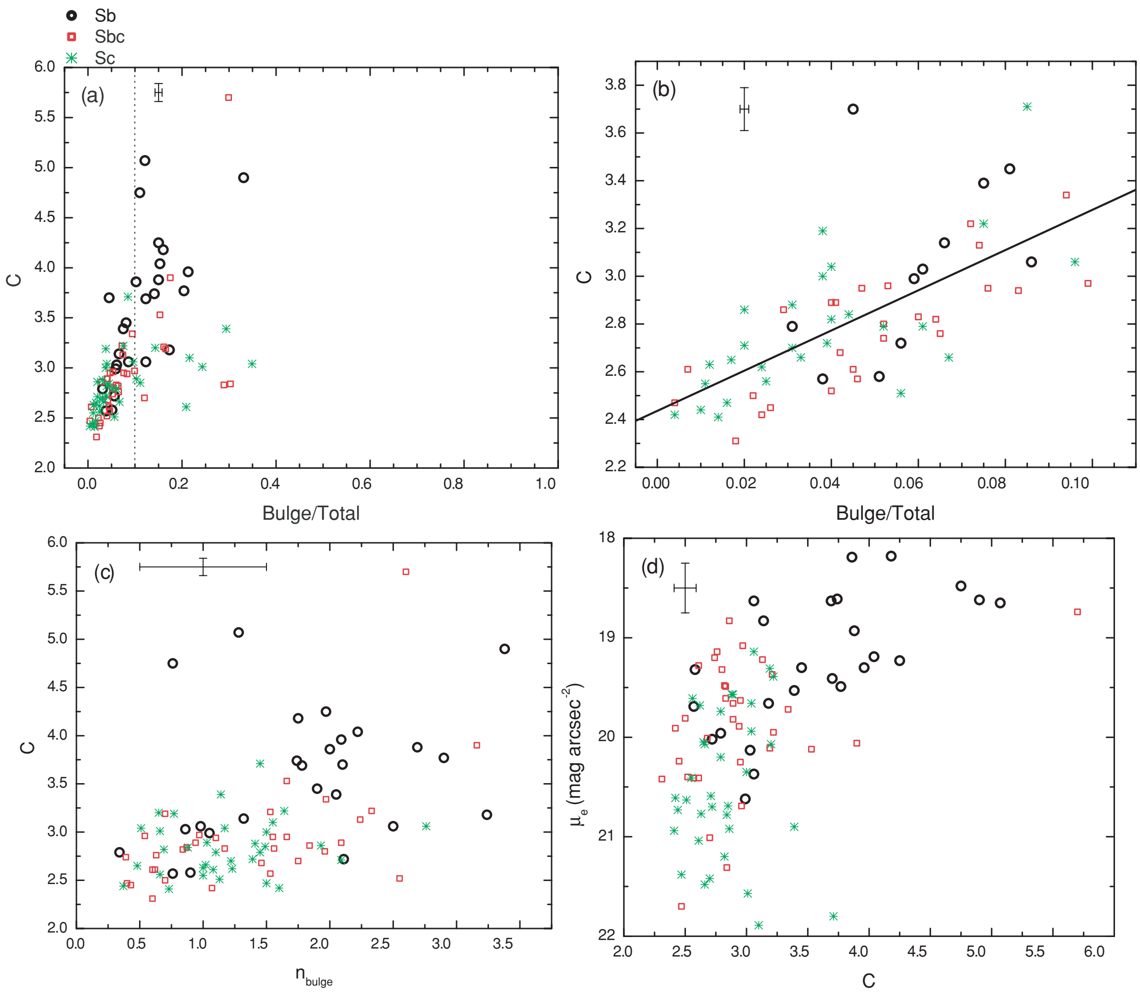

Figure 12. Concentration index C shown in relation to parameters describing the bulge: bulge/total luminosity ratio (a–b), Sérsic index $n_{\rm bulge}$ (c) and bulge effective surface brightness $\mu_{\rm e}$ (d). Panel (b) offers a detailed look at C versus bulge/total from panel (a), with an emphasis on the region to the left-hand side of bulge/total = 0.1, denoted by the vertical dotted line in (a). The three morphological types are indicated with different symbols (see figure's legend). The typical 2σ errorbars are shown in each panel.

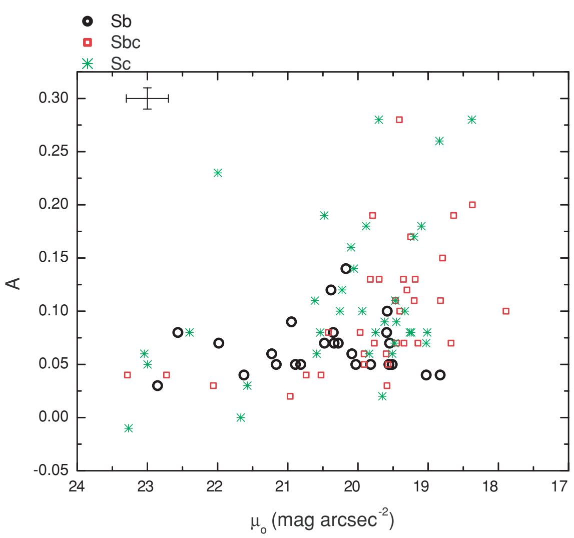

Figure 13. Asymmetry index A in relation to disc central surface brightness $\mu_{\rm o}$. The three morphological types are indicated with different symbols (see figure's legend). The typical 2σ errorbars are shown.

1979, 1993; Norman, Sellwood & Hasan 1996; Hasan, Pfenniger & Norman 1998; Fathi & Peletier 2003; Kormendy & Kennicutt 2004; Athanassoula 2005; Jogee, Scoville & Kenney 2005; Debattista et al. 2006). Others have suggested that bars can help the process of 'pseudo-bulge' formation (making it faster and more efficient), but is not a necessary requirement for that process (e.g. Laurikainen et al. 2007, and references therein). Bars can transport gas inward (e.g. Sakamoto et al. 1999; Sheth et al. 2005) potentially contributing to the formation of a bulge. On the other hand, it has been proposed that even without a bar the stellar disc component could be redistributed due to a secular torque action (e.g. Zhang & Buta 2007).

We find a larger fraction of barred galaxies among Sb types relative to Sbc–Sc types (Section 4.2). Sb galaxies also appear to host the largest bars (Table 6a) within the morphological sequence Sb–Sbc–Sc. If bars are assumed as necessary precursors of all pseudo-bulges, then the smaller bars in later type galaxies 'dissolve' more efficiently in the process of bulge formation. It is interesting to mention that for Sb and Sbc types in our sample of isolated galaxies, we find systematically larger values of the index $n_{\rm bulge}$ for barred galaxies compared to the non-barred galaxies (Tables 6a–b). The difference almost vanishes for Sc barred and non-barred galaxies.

Table 11. Mean/median for CAS parameters of all Sb–Sc galaxies in our sample versus the Sb–Sc nearby normal galaxies from Frei sample (Conselice 2003).

	C		A		S	
	Mean ± SE	median	Mean ± SE	median	Mean ± SE	median
This study	3.06 ± 0.06	2.89	0.09 ± 0.01	0.08	0.20 ± 0.01	0.20
Conselice (2003)	3.47 ± 0.08	3.44	0.14 ± 0.01	0.13	0.28 ± 0.02	0.25

Note: *SE* is standard deviation of the mean.
Column (1): morphological type. Column (2): C – concentration. Column (3): A – asymmetry. Column (4): S – clumpiness.

Laurikainen et al. (2007) report a rather opposite result for Sb type (see their fig. 3). If $n_{\rm bulge}$ is one of the empirical discriminators between classical and pseudo-bulges then any connection with the presence/absence of bars merits further attention. In this context, it is relevant to review our Figs 8(a)–(b). We note the 'disappearance' of objects with $n_{\rm bulge}$ above 1.7 for non-barred galaxies (Fig. 8b in contrast to Fig. 8a). We tested whether this may be caused by the resolution limitation in SDSS images, thus the BUDDA code's inability to identify the presence of a bar. First, we analysed the distribution of $n_{\rm bulge}$ values of non-barred galaxies with $V_{\rm R}$ lower and higher than the median $V_{\rm R}$ of the full non-barred sample ($\sim$5700 km s^{-1}), respectively. We found no significant difference. Secondly, for our galaxies, the typical seeing full width at half-maximum is better than 1 arcsec, with very few cases at 1.5 arcsec. Considering the most extreme case, for a galaxy showing $V_{\rm R} \simeq 10\,000$ km s^{-1}, a 1.5 arcsec seeing would translate into a spatial resolution of $\sim$1.0 kpc, which is well within the capability of the BUDDA code to provide reliable structural measures (Gadotti 2008). The scarcity of non-barred galaxies with $n_{\rm bulge}$ above 1.7 is consistent with the scenario that bars could transform by dissolution into pseudo-bulges. The presence of bars may influence the degree of relaxation of bulges in the sense that $n_{\rm bulge}$ decreases from Sb through Sc only for barred galaxies, but not for non-barred spirals (Section 4.2).

The formation and lifetime of bars may be sensitive to environment (e.g. Gerin, Combes & Athanassoula 1990). It has been suggested that bars in early-type spiral galaxies are formed by tidal interactions with other galaxies and those in late types have intrinsic origin (Noguchi 1996). The connection bars environment may be different for early- and late-type spirals (Noguchi 1996, 2000), being proposed a 'bimodality' of bars in this sense. Moreover, numerical simulations have shown that for Sb–Sc galaxies bars are transient features and dissolve progressively in $\sim$1–2 Gyr (Bournaud, Combes & Semelin 2005). As we pointed out earlier, the AMIGA/CIG isolated galaxies have been basically nurture-free for at least a comparable time. We find that $\sim$50–60 per cent of our present sample is barred galaxies. The conclusion here could be that the bars we observe in these late-type isolated spiral galaxies have been likely renewed or reformed through internal processes and not by external accretion or interactions (e.g. Block et al. 2002; Berentzen et al. 2004). It is also interesting to mention we find that the largest bars lie in discs with the lowest central surface brightness $\mu_{\rm o}$ (Fig. 9b). This is consistent with the idea that bars build up from the material in the central parts of discs and they are products of secular dynamical evolution within the disc.

We find that our isolated galaxies tend to host large bars.[10] Our Fig. 6 shows that most bar radii are clustered in the range 2–6 kpc. Erwin 2005 (based on Martin 1995) reports typical bar sizes in the range 1–3 kpc (*B* band) for morphological types Sb–Sc having absolute magnitudes similar to our sample. A more recent study (Marinova & Jogee 2007) presents a characterization of bars in optical (*B* band) and near-IR (*H* band) for the OSUBSGS sample of galaxies. In order to compare the bar sizes with their estimates, we restrict their sample to Sb–Sc morphological range, based on the RC3 catalogue (de Vaucouleurs et al. 1991). The OSUBSGS-based sample has a similar distribution of absolute magnitudes as our sample. In terms of $l_{\rm bar}$, our sample of barred galaxies (n = 48) is characterized by a mean $\sim$5.0 kpc and a median $\sim$4.8 kpc. For the OSUBSGS sample of $n = 49$ barred galaxies, the mean and median values (*H* band) of $l_{\rm bar} \sim 3.8$ and $\sim$3.4 kpc, respectively. The conclusion is that the size of bars may be related to the environment, isolation favouring larger bars.

Moreover, this conclusion seems to be consistent with reports that the disc scalelength $h_{\rm R}$ of spiral galaxies in rich environments is typically smaller than that of field (i.e. isolated) galaxies (e.g. Aguerri et al. 2004). We find that the bar size scales with the disc scalelength $h_{\rm R}$ (our Fig. 9; see also Laine et al. 2002). In extreme environments (e.g. compact groups), spiral galaxies tend to lose their disc components by dissolution into a stellar halo. The size of the discs in what we assumed was initially late-type spiral galaxies in Seyfert's Sextet for example (estimated by the last concentric isophote) is less than 10 kpc diameter, comparable to the smallest discs in our present sample (Durbala et al. 2008). Comparing our $l_{\rm bar}/a^i_{25}$ estimates with the similar quantities reported in Erwin (2005), we observe the same declining trend from Sb through Sc; for our sample we do obtain systematically larger $l_{\rm bar}/a^i_{25}$ ratios relative to that study, although we note that Erwin (2005) measures are based on *B*-band data from Martin (1995).

7.3 CAS structural measures in isolated galaxies

The minimal environmental influence on AMIGA/CIG galaxies investigated here is revealed also by an analysis of the structural properties in terms of CAS parameters (Section 5). Due to the narrow morphological range represented in our sample of isolated galaxies, any attempt at comparison with other studies must be cautiously explored. None the less, the size of the sample examined in this study allows a meaningful comparison of the 96 galaxies as a whole (i.e. the full set of Sb–Sc galaxies) with galaxies of same morphological types selected without isolation constraints. Table 11 offers such a comparison with the subsample of Sb–Sc galaxies ($n = 49$) examined in Conselice (2003), extracted from the Frei, Guhathakurta & Gunn (1996) sample, assumed representative for the population of nearby normal galaxies. The general conclusion is that the isolated galaxies are less concentrated, less asymmetric and less clumpy than other galaxies of same morphological type selected without isolation criteria. Thus, we may have clear indications of environmental

[10] However, one must be aware that there is no standard definition for the length of a bar in a galaxy (Erwin 2005) and scaling parameters for galaxy components may be sensitive to the filter that is used for photometry.

influence on the structure of galaxies. This may be telling us that the formation of large central concentrations and large clumps within discs is disfavoured in the absence of comparable sized neighbours.

7.4 Describing the morphological classification

Although our study involves a narrow range of morphological types, all plots that involve exclusively bulge measures show clear morphological separation (e.g. Fig. 5). When we combine disc measures (e.g. Fig. 7a), the morphological segregation is less clear or absent suggesting some commonality among disc properties over the Sb–Sc range. Thus, it appears that the morphological separation may be associated with a change in the luminosity profile of bulges as indicated by their Sérsic indices. Hunt et al. (2004) proposed that spiral galaxies may begin with low bulge Sérsic index. As they age, they change into structurally more evolved systems (towards $n_{\rm bulge} = 4$ or higher) also characterized by higher surface brightness (see Figs 5a and 12d) and an increased absolute magnitude (see Figs 5b–d). However, Carollo (1999) argue that pseudo-bulges cannot evolve into denser $r^{1/4}$ (i.e. $n_{\rm bulge} = 4$) bulges just by repeated cycles of bar formation/disruption.

At the same time, one should keep in mind that the bulge Sérsic index is associated with rather large uncertainties (Section 4.1), which complicates its use for a quantitative morphological classification (Gadotti 2008). It appears that the concentration index C, the bulge/total (or bulge/disc) luminosity ratio and the bulge Sérsic index are relevant parameters when one describes the morphological sequence of spiral galaxies from earlier to later types. None the less, Fig. 12 suggests that the morphological diversity of spiral galaxies is deeply connected to the structure of their bulges. The concentration index C is not a good tracer of bulge/total ratio for bulge/total > 0.1. This is true because the bulge light is no longer concentrated within the radius that includes 20 per cent of the total light (Section 3; see also Graham 2001b). It is not obvious why the bulge surface brightness shows a plateau in its trend versus C (Fig. 12d). However, one may speculate that the fact that some of the Sb galaxies curve away from the main trend (described largely by Sbc and Sc types) towards larger C values could be due to a different type of bulges they host.

7.5 Final remarks

This study could be complemented by an extension of a similar type of analysis to the whole set of isolated spiral galaxies, which would include the whole sequence of Hubble morphological types. This would provide a more general and clear picture on the morphological type dependence of various structural properties and scaling relations presented and discussed here. Measures of bulge colours and kinematics would both provide strong tests of our hypothesis that most isolated spirals involve pseudo-bulges. Another complementary approach is a Fourier analysis of our images, which would provide a quantitative description of the spiral structure, intimately connected to galactic morphology as well. This is part of an ongoing project we are working on at this time and the results will be presented in a future paper.

ACKNOWLEDGMENTS

We thank Dr Dimitri Alexei Gadotti for answering many questions about the BUDDA code. His prompt and clear replies are sincerely appreciated. LVM is partially supported by DGI Grant AYA 2005-07516-C02-01 and Junta de Andalucía (Spain).

This study has made use of SDSS DR6. Funding for the SDSS and SDSS-II has been provided by the Alfred P. Sloan Foundation, the Participating Institutions, the National Science Foundation, the US Department of Energy, the National Aeronautics and Space Administration, the Japanese Monbukagakusho, the Max Planck Society and the Higher Education Funding Council for England. The SDSS web site is http://www.sdss.org/. The SDSS is managed by the Astrophysical Research Consortium for the Participating Institutions. The Participating Institutions are the American Museum of Natural History, Astrophysical Institute Potsdam, University of Basel, University of Cambridge, Case Western Reserve University, University of Chicago, Drexel University, Fermilab, the Institute for Advanced Study, the Japan Participation Group, Johns Hopkins University, the Joint Institute for Nuclear Astrophysics, the Kavli Institute for Particle Astrophysics and Cosmology, the Korean Scientist Group, the Chinese Academy of Sciences (LAMOST), Los Alamos National Laboratory, the Max-Planck-Institute for Astronomy (MPIA), the Max-Planck-Institute for Astrophysics (MPA), New Mexico State University, Ohio State University, University of Pittsburgh, University of Portsmouth, Princeton University, the United States Naval Observatory and the University of Washington.

REFERENCES

Adelman-McCarthy J. K. et al., 2008, ApJS, 175, 297
Aguerri J. A. L., Balcells M., Peletier R. F., 2001, A&A, 367, 428
Aguerri J. A. L., Iglesias-Paramo J., Vilchez J. M., Muñoz-Tuñón C., 2004, AJ, 127, 1344
Andredakis Y. C., Sanders R. H., 1994, MNRAS, 267, 283
Andredakis Y. C., Peletier R. F., Balcells M., 1995, MNRAS, 275, 874
Athanassoula E., 2005, MNRAS, 358, 1477
Barazza F. D., Jogee S., Marinova I., 2008, ApJ, 675, 1194
Baugh C. M., Cole S., Frenk C. S., 1996, MNRAS, 283, 1361
Beijersbergen M., de Blok W. J. G., van der Hulst J. M., 1999, A&A, 351, 903
Berentzen I., Athanassoula E., Heller C. H., Fricke K. J., 2004, MNRAS, 347, 220
Bershady M. A., Jangren A., Conselice C. J., 2000, AJ, 119, 2645
Block D. L., Bournaud F., Combes F., Puerari I., Buta R., 2002, A&A, 394, 35
Bournaud F., Combes F., Semelin B., 2005, MNRAS, 364, L18
Buta R. J., Corwin H. G., Jr, Odewahn S. C., 2007, The de Vaucouleurs Atlas of Galaxies. Cambridge Univ. Press, Cambridge (ISBN-13 978-0-521-82048-6)
Capaccioli M., Caon N., D'Onofrio M., 1992, MNRAS, 259, 323
Carlberg R. G., 1999, in Carollo C. M., Ferguson H. C., Wyse R. F. G., eds, The Formation of Galactic Bulges. Cambridge Univ. Press, Cambridge, p. 64
Carollo C. M., 1999, ApJ, 523, 566
Cole S., Lacey C. G., Baugh C. M., Frenk C. S., 2000, MNRAS, 319, 168
Combes F., Elmegreen B. G., 1993, A&A, 271, 391
Conselice C. J., 2003, ApJS, 147, 1
Conselice C. J., Bershady M. A., Jangren A., 2000, ApJ, 529, 886
Courteau S., de Jong R. S., Broeils A. H., 1996, ApJ, 457, L73
Debattista V. P., Carollo C. M., Mayer L., Moore B., 2004, ApJ, 604, L93
Debattista V. P., Mayer L., Carollo C. Marcella, Moore B., Wadsley J., Quinn T., 2006, ApJ, 645, 209
de Jong R. S., 1996, A&AS, 118, 557
de Souza R. E., Gadotti D. A., dos Anjos S., 2004, ApJS, 153, 411
de Vaucouleurs G., 1948, Ann. Astrophys., 11, 247
de Vaucouleurs G., de Vaucouleurs A., Corwin H. G., Jr, Buta R. J., Paturel G., Fouque P., 1991, Third Reference Catalog of Bright Galaxies. New York, Springer (RC3)
Djorgovski S., Davis M., 1987, ApJ, 313, 59
Drory N., Fisher D. B., 2007, ApJ, 664, 640

Durbala A. et al., 2008, AJ, 135, 130
Eggen O. J., Lynden-Bell D., Sandage A. R., 1962, ApJ, 136, 748
Eliche-Moral M. C., Balcells M., Aguerri J. A. L., González-García A. C., 2006, A&A, 457, 91
Elmegreen B. G., Elmegreen D. M., 1985, ApJ, 288, 438
Erwin P., 2005, MNRAS, 364, 283
Eskridge P. B. et al., 2000, AJ, 119, 536
Eskridge P. B. et al., 2002, ApJS, 143, 73
Espada D., 2006, PhD thesis, Instituto de Astrofísica de Andalucía
Espada D., Bosma A., Verdes-Montenegro L., Athanassoula E., Leon S., Sulentic J., Yun M. S., 2005, A&A, 442, 455
Faber S. M., Jackson R. E., 1976, ApJ, 204, 668
Faber S. M., Dressler A., Davies R. L., Burstein D., Lynden-Bell D., 1987, Proc. the Eighth Santa Cruz Summer Workshop in Astronomy and Astrophysics. Springer-Verlag, New York, p. 175
Fathi K., Peletier R. F., 2003, A&A, 407, 61
Fisher D. B., Drory N., 2008, AJ, 136, 773
Freeman K. C., 1970, ApJ, 160, 811
Frei Z., Guhathakurta P., Gunn J. E., Tyson J. A., 1996, AJ, 111, 174
Fukugita M., Ichikawa T., Gunn J. E., Doi M., Shimasaku K., Schneider D. P., 1996, AJ, 111, 1748
Gadotti D. A., 2008, MNRAS, 384, 420
Gerin M., Combes F., Athanassoula E., 1990, A&A, 230, 37
Gil de Paz A. et al., 2007, ApJS, 173, 185
Graham A. W., 2001a, MNRAS, 326, 543
Graham A. W., 2001b, AJ, 121, 820
Graham A. W., 2002, MNRAS, 334, 721
Graham A. W., de Blok W. J. G., 2001, ApJ, 556, 177
Graham A. W., Worley C. C., 2008, MNRAS, 388, 1708
Grosbøl P. J., 1985, A&AS, 60, 261
Gunn J. E. et al., 1998, AJ, 116, 3040
Gunn J. E. et al., 2006, AJ, 131, 2332
Hamabe M., Kormendy J., 1987, in de Zeeuw P. T., ed., Proc. IAU Symp. 127, Structure and Dynamics of Elliptical Galaxies. Reidel, Dordrecht, p. 379
Hasan H., Pfenniger D., Norman C. A., 1998, BAAS, 30, 1408
Ho L. C., Filippenko A. V., Sargent W. L. W., 1997, ApJ, 487, 591
Hogg D. W., Finkbeiner D. P., Schlegel D. J., Gunn J. E., 2001, AJ, 122, 2129
Hunt L. K., Pierini D., Giovanardi C., 2004, A&A, 414, 905
Isobe T., Feigelson E. D., Akritas M. G., Babu G. J., 1990, ApJ, 364, 104
Jogee S., Scoville N., Kenney J. D. P., 2005, ApJ, 630, 837
Karachentseva V. E., 1973, Astrofiz. Issled.-Izv. Spets. Astrofiz. Obs., 8, 3
Kauffmann G., 1996, MNRAS, 281, 487
Kent S. M., 1985, ApJS, 59, 115
Khosroshahi H. G., Wadadekar Y., Kembhavi A., 2000, ApJ, 533, 162
Knapen J. H., 1999, in Beckman J. E., Mahoney T. J., eds, ASP Conf. Ser. Vol. 187, The Evolution of Galaxies on Cosmological Time-scales. Astron. Soc. Pac., San Francisco, p. 72
Kormendy J., 1979, ApJ, 227, 714
Kormendy J., 1985, ApJ, 295, 73
Kormendy J., 1993, in Dejonghe H., Habing H. J., eds, Proc. IAU Symp. 153, Galactic Bulges. Kluwer, Dordrecht, p. 209
Kormendy J., Kennicutt R. C., Jr, 2004, ARA&A, 42, 603
Laine S., Shlosman I., Knapen J. H., Peletier R. F., 2002, ApJ, 567, 97
Larson R. B., Tinsley B. M., 1978, ApJ, 219, 46
Laurikainen E., Salo H., Buta R., Vasylyev S., 2004, MNRAS, 355, 1251
Laurikainen E., Salo H., Buta R., Knapen J. H., 2007, MNRAS, 381, 401
Leon S., Verdes-Montenegro L., 2003, A&A, 411, 391
Leon S. et al., 2008, A&A, 485, 475
Lisenfeld U. et al., 2007, A&A, 462, 507
Lupton R. H., Gunn J. E., Ivezic Z., Knapp G. R., Kent S., Yasuda N., 2001, in Harnden F. R., Jr, Primini F. A., Payne H. E., eds, ASP Conf. Ser. Vol. 238, Astronomical Data Analysis Software and Systems X. Astron. Soc. Pac., San Francisco, p. 269
MacArthur L. A., Courteau S., Holtzman J. A., 2003, ApJ, 582, 689
McCall M. L., 2004, AJ, 128, 2144
Marinova I., Jogee S., 2007, ApJ, 659, 1176
Martin P., 1995, AJ, 109, 2428
Menéndez-Delmestre K., Sheth K., Schinnerer E., Jarrett T. H., Scoville N. Z., 2007, ApJ, 657, 790
Méndez-Abreu J., Aguerri J. A. L., Corsini E. M., Simonneau E., 2008, A&A, 478, 353
Merlin E., Chiosi C., 2006, A&A, 457, 437
Noguchi M., 1996, ApJ, 469, 605
Noguchi M., 2000, MNRAS, 312, 194
Norman C. A., Sellwood J. A., Hasan H., 1996, ApJ, 462, 114
Pier J. R., Munn J. A., Hindsley R. B., Hennessy G. S., Kent S. M., Lupton R. H., Ivezić, Ž., 2003, AJ, 125, 1559
Roberts M. S., Haynes M. P., 1994, ARA&A, 32, 115
Sabater J., Leon S., Verdes-Montenegro L., Lisenfeld U., Sulentic J., Verley S., 2008, A&A, 486, 73
Sakamoto K., Okumura S. K., Ishizuki S., Scoville N. Z., 1999, ApJ, 525, 691
Sandage A., Tammann G. A., 1981, A Revised Shapley-Ames Catalog of Bright Galaxies, 1st edn. Carnegie Institute of Washington
Schlegel D. J., Finkbeiner D. P., Davis M., 1998, ApJ, 500, 525
Sérsic J. L., 1968, Atlas de Galaxias Australes. Observatorio Astronomico, Cordoba
Shen S., Mo H. J., Shu C., 2002, MNRAS, 331, 259
Sheth K., Vogel S. N., Regan M. W., Thornley M. D., Teuben P. J., 2005, ApJ, 632, 217
Shimasaku K. et al., 2001, AJ, 122, 1238
Smith J. A. et al., 2002, AJ, 123, 2121
Stoughton C. et al., 2002, AJ, 123, 485
Sulentic J. W. et al., 2006, A&A, 449, 937
Takamiya M., 1999, ApJS, 122, 109
Taylor-Mager V. A., Conselice C. J., Windhorst R. A., Jansen R. A., 2007, ApJ, 659, 162
Thomas D., Davies R. L., 2006, MNRAS, 366, 510
Tully R. B., Mould J. R., Aaronson M., 1982, ApJ, 257, 527
van den Bergh S., 1960a, ApJ, 131, 215
van den Bergh S., 1960b, ApJ, 131, 558
van den Bosch F. C., 1998, ApJ, 507, 601
Verdes-Montenegro L., Sulentic J., Lisenfeld U., Leon S., Espada D., Garcia E., Sabater J., Verley S., 2005, A&A, 436, 443
Verley S. et al., 2007a, A&A, 470, 505
Verley S. et al., 2007b, A&A, 472, 121
Verley S., Combes F., Verdes-Montenegro L., Bergond G., Leon S., 2007c, A&A, 474, 43
Wyse R. F. G., 1982, MNRAS, 199, 1
Zhang X., 2004, in Ryder S. D., Pisano D. J., Walker M. A., Freeman K. C., eds, Proc. IAU Symp. Vol. 220, Dark Matter in Galaxies. Astron. Soc. Pac., San Francisco, p. 417
Zhang X., Buta R. J., 2007, AJ, 133, 2584

This paper has been typeset from a TEX/LATEX file prepared by the author.